A ribosomopathy reveals decoding defective ribosomes driving human dysmorphism

Nahuel A. Paolini[1,10], Martin Attwood[2,10], Samuel B. Sondalle[3,10], Carolina Marques dos Santos Vieira[4,10], Anita M. van Adrichem[5], Franca M. di Summa[1], Marie-Françoise O'Donohue[6], Pierre-Emmanuel Gleizes[6], Swaksha Rachuri[4], Joseph W. Briggs[4], Roman Fischer[2], Peter J. Ratcliffe[2], Marcin W. Wlodarski[7], Riekelt H. Houtkooper[5], Marieke von Lindern[1], Taco W. Kuijpers[8], Jonathan D. Dinman[4], Susan J. Baserga[9], Matthew E. Cockman[2], Alyson W. MacInnes[1,5]*

[1] Department of Hematopoiesis, Sanquin and Landsteiner Laboratory, AMC/UvA, 1066 CX Amsterdam, The Netherlands.
[2] Target Discovery Institute, University of Oxford, Oxford, OX3 7FZ, UK
[3] Department of Genetics, Yale University School of Medicine, New Haven, CT 06520, USA
[4] Department of Cell Biology and Molecular Genetics, University of Maryland, College Park, MD 20742, USA
[5] Laboratory of Genetic Metabolic Diseases, Academic Medical Center, 1105 AZ Amsterdam, The Netherlands
[6] Laboratoire de Biologie Moléculaire Eucaryote, CNRS, Université Paul Sabatier, Toulouse, France
[7] Department of Pediatric Hematology and Oncology, University of Freiburg, 79110 Freiburg, Germany
[8] Department of Pediatric Hematology, Immunology and Infectious Diseases, Emma Children's Hospital, Academic Medical Center, 1105 AZ Amsterdam, The Netherlands
[9] Department of Molecular Biophysics and Biochemistry, Genetics, and Therapeutic Radiology, Yale University School of Medicine, New Haven, CT, USA
[10] Equal Contribution
* Corresponding author: a.w.macinnes@amc.nl

Abstract

Ribosomal protein (RP) gene mutations, mostly associated with inherited or acquired bone marrow failure, are believed to drive disease by slowing the rate of protein synthesis. Here *de novo* missense mutations in the *RPS23* gene, which codes for uS12, are reported in two unrelated individuals with microcephaly, hearing loss, and overlapping dysmorphic features. One individual additionally presents with intellectual disability and autism spectrum disorder. The amino acid substitutions lie in two highly conserved loop regions of uS12 with known roles in maintaining the accuracy of mRNA codon translation. Primary cells revealed one substitution severely impaired OGFOD1-dependent hydroxylation of a neighboring proline residue resulting in 40S ribosomal subunits that were blocked from polysome formation. The other disrupted a predicted pi-pi stacking interaction between two phenylalanine residues leading to a destabilized uS12 that was poorly tolerated in 40S subunit biogenesis. Despite no evidence of a reduction in the rate of mRNA translation, these uS12 variants impaired the accuracy of mRNA translation and rendered cells highly sensitive to oxidative stress. These discoveries describe a ribosomopathy linked to uS12 and reveal mechanistic distinctions between RP gene mutations driving hematopoietic disease and those resulting in developmental disorders.

Introduction

Ribosomopathies are diseases caused by mutations in genes coding for components of the ribosome, such as ribosomal proteins (RPs), or in one of the many proteins required for ribosome biogenesis and maturation. Classical ribosomopathies have been typically associated with bone marrow failure (BMF). Examples are the inherited BMF Diamond-Blackman anemia (DBA) (OMIM #105650) and acquired 5q-myelodysplastic syndrome (5q-MDS) (OMIM #153550), both of which are linked to RP gene haploinsufficiency and predominantly effect the development of red blood cells[1; 2]. Other inherited BMF syndromes linked to genes important for ribosome biogenesis are dyskeratosis congenita (OMIM #305000) and Shwachman-Diamond syndrome (OMIM #260400), diseases that drive pancytopenia and neutropenia, respectively.

Beyond the hematopoietic phenotype of ribosomopathies are developmental disorders. Almost 30% of individuals diagnosed with DBA experience physical malformations of the hands (such as abnormal thumbs), face (low nasal bridge, cleft lip/palate), head (microcephaly), heart, or urogenitals[1]. Treacher-Collins syndrome (OMIM #154500) is a disorder associated with mutations affecting rRNA production that affects development of the facial bones, eyes, and ears. Isolated congenital asplenia (ICA) (OMIM #271400) is linked to extremely rare mutations of the gene coding for ribosomal protein uS2 (RPSA)[3]. Mutations in the gene coding for ribosomal protein uL16 (RPL10) (OMIM #300847) are found in individuals with intellectual disability (ID), autism spectrum disorder (ASD), and cerebellar hypoplasia. These individuals also present with microcephaly, anteverted ears, a broad nasal ridge and epicanthus, myopia, urogenital anomalies, and a delay of motor development[4-6]. While almost all DBA-linked RP gene mutations studied to date are loss of function[7], the fact that inherited variants of uS2 and uL16 exist in the absence of any hematopoietic phenotype suggests more mechanisms underlying the pathogenicity of these mutations remain to be uncovered. Further support for this comes from the discovery that somatic mutations in genes coding for uL16 and uL18 (RPL5) are associated with the malignancy T-cell acute lymphoblastic leukemia[8].

Here *de novo* missense mutations in the *RPS23* gene coding for ribosomal protein uS12 were investigated in two unrelated individuals with microcephaly, hearing loss, and overlapping dysmorphic features. uS12 is positioned within the decoding center of the ribosome that serves to maintain translational fidelity by monitoring the complementarity between the mRNA codons being translated and the anti-codons of aminoacyl-tRNAs[9]. Studies in yeast and bacteria have described several amino acid substitutions within two highly conserved loop regions in uS12, PNSA and PGVRY, which disrupt translational fidelity and impair the accuracy of mRNA decoding[10-12].

Human uS12 is a known substrate of the 2-oxoglutarate and Fe(II)-dependent oxygenase domain-containing protein 1 (OGFOD1)[13]. Acute reductions of OGFOD1 in mammalian cells alter translational fidelity and increase the formation of mRNA-containing stress granules[13]. This study uncovers similar phenotypes in human cells carrying *RPS23* mutations that lead to uS12 variants in the PNSA and PGVRY domains. Moreover, the results suggest that the mutations impair OGFOD1 hydroxylation and stabilization of uS12, and that a mechanism exists in cells preventing ribosomes carrying the uS12 variant from entering the translationally-active polysomal pool.

Materials and Methods

Cell culture. Fibroblasts were obtained by a punch biopsy and maintained in DMEM (Gibco) + 10% FCS and 1% penicillin/streptomycin. LCLs were derived from EBV-immortalization of peripheral mononuclear cells isolated from whole blood using Ficoll (GE Life Sciences) and grown in RPMI (Gibco) + 10% FCS + 1% L-glutamine + 1% penicillin/streptomycin as previously described[14]. The study was approved by the Medical Ethical Committee (METC) of the Amsterdam Medical Center (AMC) and performed in accordance with the ethical standards of the 1964 Declaration of Helsinki. Written informed consent was received from the participants prior to inclusion in this study.

Exome sequencing. Whole exome sequencing was performed with a SOLiDv4 machine from Life TechnologiesTM after enrichment with the Agilent SureSelectXT Human All Exon 50Mb Kit. Data analysis was done with BioScopeTM. The analysis in this indication was focused on identification of *de novo* variants. Comparing the exome data of the individual with the exome data of both parents identified the de novo variants. Sanger sequencing confirmed the variants in uS12.

Sanger sequencing of fibroblasts. cDNA was synthesized using the QuantiTect reverse transcription kit (Qiagen #205313). The *RPS23* gene was amplified by standard PCR using 250 ng of cDNA and with forward primer 5'-TGCGGTGCTTCTCTCTTTCG-3' and reverse primer 5'- CATCTTGGGCCCCTGTAAGA-3'. Unincorporated primers and dNTPs were eliminated with ExoSAP-IT (Fisher Scientific #AF8200200). A BigDye Terminator sequence reaction was performed according to the manufacturer's instructions in a total reaction volume of 10µl using sequencing primer 5'- GTCACCGACGAGACCAGAAG-3'. Sequences were analyzed with 3730XL DNA Analyzer (ThermoFisher Scientific #3730XL) and 4Peaks software.

Ribosome purification. uS12 was isolated from intact ribosomes by sucrose density sedimentation and purified by reverse-phase HPLC using established protocols[13]. uS12-

containing fractions were lyophilised by vacuum centrifugation prior to solubilization in Laemmli buffer, resolution by SDS-PAGE with Coomassie Blue visualization (Imperial Protein Stain, Thermo Fisher) and in-gel trypsinolysis (Trypsin Singles, Sigma).

RNA sequencing. Total RNA was isolated from $1x10^6$ of healthy control or uS12 p.Arg67Lys LCLs using TRIzol (Thermo Fisher) and purified by Qiagen RNAeasy columns (Qiagen). RNA-Seq libraries were prepared using poly(A)+ selection of the mRNA. Unstranded RNA-Seq was performed using HiSeq 2000 v4 Paired-End 125bp protocol. The transcripts were pseudo-aligned and quantified using Kallisto. Expression levels were expressed as Fragments Per Kilobase of transcript per Million mapped reads (FPKM).

Mass spectrometry. Liquid chromatography was performed on a Dionex Ultimate 3000 nanoLC system employing a trapping configuration (Pepmap 100, C18, 5um, 100um x 2cm, Thermo Fisher) with 8ul/min flow. Separation was performed with 250 nl/min flowrate on a gradient of 2% to 35% ACN in 0.1% Formic acid and 5% DMSO over 60 minutes on an Easyspray column (Pepmap RSLC, C18, 2um, 75mm x 50cm, Thermo Fisher) with mass spectrometric analysis on an Orbitrap Fusion Lumos mass spectrometer. MS1 scans were acquired between 360 and 1500 m/z with a resolution of 120,000 for up to 50ms and an ion target of 4E5. We acquired an MS1 scan every 3 seconds and used the parallelizable time to maximize MS2 scan events in the linear ion trap (rapid scan, CID with 35% collision energy) for up to 250ms and an ion target of 4E3. Dynamic precursor exclusion was set to 7 seconds and the precursor selection threshold was 5E3 counts after quadrupole isolation (1.2 m/z). Data processing was performed using PEAKS 7 software (Bioinformatics Solutions) with the following parameters: full tryptic specificity with two missed cleavages; mass tolerance set at 5 ppm for precursor and 0.5 Da for product ions; cysteine carbamidomethylation as a fixed modification; methionine oxidation, hydroxylation, deamidation (Asn/Gln) and Pyro-glu (Gln) were specified as variable modifications; and a maximum of 3 PTMs per peptide. Unspecified PTM searches were enabled *via* PEAKS PTM algorithm. Data files were searched against human Uniprot database (release 2016_01) supplemented with the uS12 p.Arg67Lys protein

sequence. Peptide assignments were filtered to a false discovery rate (FDR) of ≤ 1% and a peptide score (-10 lgP) of ≥ 15. PEAKS searches assigned a number of modifications associated with sample handing to Pro62 containing peptides, including: conversion of N-terminal Gln to pyro-Glu, deamidation of Gln/Asn and carbamylation and carbamidomethylation of Lys. Since detection of these artifactual modifications varied between samples, we measured the most frequently detected peptide variants and aggregated the data in order to derive a robust quantitation (Table S1 for summary of quantitated peptides and counts). Relative peptide quantitation was performed using precursor ion signal intensity. Abundance measurements (peak area integrations of extracted ion chromatograms) were obtained using the Genesis peak detection algorithm in Qual Browser (Xcalibur, Thermo Fisher). Where necessary, manual integrations were performed. Peptides assigned by MS/MS in at least one sample were used to derive accurate mass and retention time (AMT) signatures of precursor ions for quantitation in all samples. Stringent tolerances for AMT assignment were employed (m/z window +/- 5 ppm and 0.5 min retention time deviation) reflecting the high mass accuracy and reproducible chromatography of the nanoLC Lumos platform.

Immunoprecipitations. Endogenous OGFOD1/uS12 protein associations were assayed by OGFOD1 IP/IB (Sigma #HPA003215) and uS12 IB (Abcam # ab57764) using standard immunoprecipitation protocols. Normal rabbit IgG (Cell signaling #2729) served as control antibody for immunoprecipitation. Interactions between ectopic FLAG-OGFOD1[13] and HA-uS12 variants were assayed by transient transfection and immunoprecipitation in HEK293 cells. OGFOD1- and uS12-bound complexes were purified with anti-FLAG (Sigma) and anti-HA (Sigma) agarose affinity gel and immunoblotted with the respective epitope tag specific antibody.

Plasmids and transfections. 3xFLAG-OGFOD1 was constructed as previously described[13]. Wild type and p.Arg67Lys human *RPS23* gene fragments (NCBI CCDS47241) with a C-terminal HA tag and 5’ BamHI/3’ XbaI restriction enzyme sites were purchased from Eurofins

Genomics. These fragments were cloned into the pCS2+ vector and transfected into HEK293 cells by calcium phosphate precipitation. The p.Phe120Ile substitution was introduced into the HA-tagged wild-type uS12 pCS2+ plasmid with forward primer 5'-CTGGAGTCCGCATTAAGGTTGTC-3' and reverse primer 5'-GACAACCTTAATGCGGACTCCAG-3' using Quickchange II Site Directed Mutagenesis kit (Agilent).

Yeast plasmids and strains. A *GAL::RPS23A rps23b*Δ yeast strain was generated in the parental strain YPH499 (*MATa ura3-52 lys2-801 ade2-101 trp1-Δ63 his3-Δ200 leu2-Δ1*). The endogenous *RPS23B* locus was knocked out with the *HIS3MX6* gene amplified by the polymerase chain reaction (PCR) (oligonucleotides F-deltaB and R-deltaB) with 60 base pair ends homologous to the *RPS23B* locus from the pFA6a-HIS3MX6 plasmid[15] to create an *rps23b*Δ*::HIS3MX6* strain in YPH499. The strain was confirmed by PCR from genomic DNA using oligonucleotides F-5'rps23b and R-inhis5 (272 base pair product) as well as oligonucleotides F-inhis5 and R-3'rps23b (334 base pair product) to confirm insertion of the *HIS3MX6* gene into the *RPS23B* locus. The *rps23b*Δ strain was used to generate a strain where the endogenous *RPS23A* gene is under the control of a glucose-repressible, galactose-inducible (*GAL*) promoter by PCR amplification (oligonucleotides F-GAL and R-GAL) of the *GAL* promoter and the *kanMX6* selection marker from pFA6a-kanMX6-PGAL1[15] with 70 base pair ends homologous the upstream region adjacent to the transcription start site of the *RPS23A* gene. The strain was confirmed by PCR from genomic DNA using oligonucleotides F-inGAL and R-inRPS23A (221 base pair product) to confirm insertion of the *GAL* promoter upstream of *RPS23A*.

The *RPS23A* gene was cloned into a plasmid to heterologously express wild-type and mutated Rps23a protein. *RPS23A* was amplified by PCR from YPH499 genomic DNA with oligonucleotide primers nested-F and nested-R and PCR amplified subsequently with oligonucleotide primers GWF and GWR, PEG precipitated, and shuttled into the Gateway donor vector pDONR221 using a BP reaction (Life Technologies). To generate Rps23a mutant

proteins, a plasmid containing *RPS23A* was mutated with oligonucleotides MutArg69Lys, MutArg69Glu, MutArg69His, and MutLys62Arg and the Change-IT Multiple Mutation Site Directed Mutagenesis Kit (Affymetrix). The mutated plasmids were confirmed with Sanger sequencing by Genewiz. All genes encoding wild-type and mutated Rps23a were shuttled into the Gateway destination vector p424GPD-CFLAG-gw (*TRP1* marker). A stop codon at the end of the genes encoding wild-type and mutated Rps23a prevented expression of the C-terminal FLAG epitope. See Table S2 for oligonucleotide sequences.

Western blotting with yeast. To examine protein levels of wild-type and aberrant Rps23a, the YPH499 *GAL::RPS23A rps23b*Δ yeast strain was transformed with either empty vector (EV) p424GPD-CFLAG-gw or p424GPD-CFLAG-gw expressing wild-type or mutated Rps23a. Endogenous Rps23a was depleted by first growing yeast cultures to mid-log phase (OD_{600} = 0.3–0.8) in synthetic medium containing 2% galactose and 2% raffinose and lacking tryptophan (SG/R-W), and then by shifting yeast cultures to synthetic medium containing 2% dextrose and lacking tryptophan (SD-W) medium for 6 h at 30°C. Protein was then extracted by the alkaline lysis method[16]. Protein extracts (0.25 OD_{600} equivalents per lane) were separated on a 15% Tris-glycine gel by SDS-PAGE and transferred to a PVDF membrane. Expression of Rps23a was determined using an anti-RPS23 antibody (AbD Serotec, ca. no. MCA3433Z; 1:1,000 dilution; anti-mouse-HRP secondary antibody at 1:10,000). An anti-G6PDH antibody (Sigma, ca. no A9521; 1:10,000 dilution; anti-rabbit-HRP secondary antibody at 1:10,000) was used for a loading control.

Yeast growth assays. For analysis of complementation of the growth defect conferred by Rps23a wild-type and aberrant proteins, the YPH499 *GAL::RPS23A rps23b*Δ yeast strain was transformed with either empty vector (EV) or plasmids expressing wild-type or mutated Rps23a. For serial dilutions, 0.2 mL of cells at an OD600 of 1 were resuspended in 1 mL water, diluted 1/10 and spotted onto SG/R-W (endogenous and plasmid-borne Rps23a expressed) or SD-W (only plasmid-borne Rps23a expressed). Cells were incubated at 30 °C.

qPCR. RNA was extracted from fibroblasts grown to 70-90% confluency using TRIzol® RNA isolation reagents (ThermoFisher Scientific, #15596018) and cDNA synthesis was performed using the QuantiTect reverse transcription kit (Qiagen, #205313) both according the manufacturer's specifications. qPCR was performed with 5ng of cDNA with 1.25µM of primers in a final volume of 8µl using LightCycler® 480 (Roche, #05015243001) and LightCycler® 480 SYBR Green I Master (Roche, #04707516001). qPCR conditions were 10 min at 95°C, followed by 45 cycles at 95°C for 10s, 60°C for 10s, and 72°C for 15s and then a melting curve at 95°C and cooling to 37°C. Primers used in this assay were: Forward uS12 5'-GGACGCCCTTTTCACTGCTA-3', Reverse uS12 5'- CTGAGGCGCCGGAGATTATT-3', Forward βactin 5'- GTCAACATGATCTGGGTC-3', Reverse βactin 5'-GGCACCAGGGCGTGATGG-3'. Experiments were repeated with three independently grown samples of each cell line.

rRNA processing analysis. Lymbloblastoid cell lines and HeLa cells were cultured in RPMI and DMEM, respectively (Gibco). These media were supplemented with 10% fetal bovine serum and 1 mM sodium pyruvate (Sigma). Different 21-mer siRNAs (Eurogentec, Seraing, Belgium), whose efficiency was verified by qPCR, were used to knock down expression of the following human mRNAs in HeLa cells: uS12 (GenBank accession number: NM_001025.4): 5'- GGGUCCAGCUGAUCAAGAAdTdT-3' (siRNA *uS12-1*), 5'-GUGGCAUGAUAAACAGUAUdTdT-3' (siRNA *uS12-2*), 5'-CAGCCUUUGUACCCAAUGAdTdT-3' (siRNA *uS12-3*) (20819938). Each siRNA solution was added at a final concentration of 500 nM to 200 µl of cell suspension (50 x 10^6 cells/ml diluted in Na phosphate buffer, pH 7.25, containing 250 mM sucrose and 1 mM $MgCl_2$). Electro-transformation was performed at 240 V with a Gene Pulser (Bio-Rad, Hercules, CA)[17]. Control HeLa cells were electro-transformed with a scramble siRNA (siRNA-negative control duplex; Eurogentec). After 10 min incubation at ambient temperature, cells were plated and grown at 37°C for 48 hours.

RNA extraction and analysis by northern blot. Total RNAs were extracted with Trizol from cell pellets containing 20-30 x 10^6 cells. The aqueous phase was further extracted with phenol-chloroform-isoamylic alcohol (25:24:1; Sigma), then with chloroform. Total RNAs were recovered after precipitation with 2-propanol. For Northern blot analyses, RNAs were dissolved in formamide, denatured for 10 min at 70°C and separated on a 1.2% agarose gel containing 1.2% formaldehyde and 1X Tri/Tri buffer (30 mM triethanolamine, 30 mM tricine, pH 7.9) (3 µg RNAs/lane). RNAs were transferred to a Hybond N^+ nylon membrane (GE Healthcare, Orsay, France) by passive transfer and cross-linked under UV light. Pre-hybridization was performed for 1 hour at 45°C in 6X SSC, 5X Denhardt's solution, 0.5% SDS, 0.9 g/ml tRNA. The 5'-radiolabeled oligonucleotide probe was incubated overnight. The sequences of the probes were: 5'-ITS1 (5'-CCTCGCCCTCCGGGCTCCGTTAATGATC-3'), ITS1-5.8S (5'-CTAAGAGTCGTACGAGGTCG-3'), ITS2 (ITS2b: 5'-CTGCGAGGGAACCCCCAGCCGCGCA-3' and ITS2d/e: 5'-GCGCGACGGCGGACGACACCGCGGCGTC-3'), 18S (5'-TTTACTTCCTCTAGATAGTCAAGTTCGACC-3'), 28S (5'-CCCGTTCCCTTGGCTGTGGTTTCGCTAGATA-3'). Membranes were washed twice for 10 min in 2X SSC, 0.1% SDS and once in 1X SSC, 0.1% SDS, and then exposed. Signals were acquired with a Typhoon Trio PhosphorImager (GE Healthcare) and quantified using the MultiGauge software.

Translational fidelity assays in yeast. Yeast cells yJD 1729 (*RPS23A*), yJD 1730 (*rps23a*-p.Lys62Arg), and yJD 1731 (*rps23a*-p.Arg69Lys) were transformed using the alkali cation method[18]. pJD376 (pYDL-LA), pJD1018 (pYDL-EST2), pJD1039 (pYDL-STN1), and pJD1041 (pYDL-EST1)[19] were used to monitor rates of -1 PRF. Rates of +1 PRF were assayed using pJD377 (pYDL-EST3). pJD431 (pYDL-UAA), and pJD432 (pYDL- UAG) were used to assay termination codon readthrough. Suppression of an AGC near-cognate serine codon or a TCT non-cognate serine codon in the firefly luciferase catalytic site was assayed using pJD642 (pYDL-TCT_{218}), and pJD643 (pYDL-AGC_{218})[20; 21]. pJD375 (pYDL-control) was used as the zero

frame dual luciferase reporter. All assays were performed in triplicate a minimum of 3 independent times. The yeast strains were grown overnight in H–tryptophan –uracil liquid media containing galactose and raffinose, and after 24 hrs media was replaced with –tryptophan –uracil liquid media containing dextrose. Yeast cells were pelleted by centrifugation, resuspended in 500 µL of lysis buffer (1× PBS pH 7.4, 1 mM PMSF), and lysates were prepared as described previously[22]. Luciferase activities were determined using 20 µL of lysate/sample using the Dual-Luciferase® Assay System and a GloMax®-Multi+ Detection System (Promega). Data were analyzed as described previously[23].

Translational fidelity in fibroblast cell lines. Fibroblasts were transfected by electroporation using a Nucleofector™ II apparatus and the Normal Human Dermal Fibroblasts Nucleofector™ kit (Amaxa™), per the manufacturer's instructions. For each transfection, 4 - 5 x 10^5 cells were mixed with 3 µg of plasmid DNA. pJD2046 (pHDL-fullCMV-UAA) was used to monitor termination codon readthrough. pJD2044 (pHDL-fullCMV-control) was used as the zero frame dual luciferase reporter. To make these constructs, the CMV promoter/enhancer was PCR amplified using pCDNA3.1(+) plasmid template and the following forward and reverse oligonucleotide primers: CMVprom-forward 5'-ACTGTCGGTACCCAGATATACGCGTTGACATTGATTATTGAC-3', CMVprom-reverse 5'-ACTGTCCTGCAGGCCAGTAAGCAGTGGGTTCTCTAG-3'. Primers were designed to have either a KpnI or PstI restriction enzyme digest site so that PCR amplicons could be digested and ligated into similarly digested pJD175f(pHDL-SV40-control), and pJD1643 (pHDL-SV40-UAA) dual luciferase reporter plasmids. All assays were performed in triplicate a minimum of 3 times. Cell lysates were prepared using passive lysis buffer (Promega) and luciferase activities were determined using the Dual-Luciferase® Assay System and a GloMax®-Multi+ Detection System (Promega), per the manufacturer's instructions 24 hours post-transfection. Data were analyzed as described above for yeast translational fidelity assays.

Structural modeling, alignments, and SNP identification. All structural models of uS12 were generated from a cryo-EM structure of the human 80S ribosome (PDB ID: 4UG0)[24] using the PyMOL Molecular Graphics System, Version 1.8 Schrödinger, LLC. Identification of polar interactions, distance measurements, and modeling of mutated residues were also performed using PyMol. Multiple protein sequence alignments were performed with ClustalX 2.1[25]. SNPs were collected from the NCBI database and the cBio Cancer Genomics Portal[26].

Growth curve. 50,000 LCLs were plated in triplicate in a 12-well dish with DMEM +10%FCS and counted daily with a CASY® Cell Counter for five days. Each well was counted in triplicate each day.

***De novo* protein synthesis measurement.** 1x10e5 LCLs were plated in 150µl methionine-free medium (DMEM containing 4,500 mg/L D-glucose, without L-glutamine, sodium pyruvate, L-methionine, and L-cysteine, Invitrogen #21013). Assays performed using the Click-iT® AHA Alexa Fluor® 488 Protein Synthesis HCS Assay (Thermo Scientific) per the manufacturer's instructions using 2% paraformaldehyde for fixation and 1:1000 dilution of AHA. Fluorescence was measured by flow cytometry using an LSR-II apparatus and analyzed with FACSDiva software (BD Biosciences).

Polysome profiling analysis. 400µg of total protein from freshly lysed cells was loaded onto 17-50% sucrose gradients as previously described[27]. The tubes were centrifuged at 4°C and at 40,000 rpm for 2 hours in a SW41 rotor (Optima L100XP ultracentrifuge; Beckman Coulter). The gradient fractions were collected at OD_{254} with a Foxy Jr. gradient collector (Teledyne Isco).

Confocal analysis. Fibroblasts were plated to 50% confluence on glass coverslips in a 24-well plate. The following day cells were treated for 30 minutes with varying concentrations of arsenite (Sigma #S7400) dissolved in DMEM + 10% FCS at 37°C. Cells were fixed for 10

minutes at RT with 2% paraformaldehyde (Sigma #P6148) in PBS and washed 2x with PBS. Cells were then permeabilized for 5 minutes at RT with 0.1% Triton X-100 (Sigma #T8787) in PBS and washed 3x with PBS. Cells were then blocked for 30 minutes at RT with 1% BSA (Sigma #A2153) in PBS and incubated with G3BP1 antibodies (BD Transduction Laboratories #611126) at a 1:100 dilution in blocking buffer at RT for 30 minutes. Cells were then incubated at RT for 30 minutes with anti-mouse immunoglobulin conjugated to biotin diluted at 1:200 in blocking buffer (Dako #E0433), followed by 2x washes with PBS and a final incubation in the dark for 30 minutes at RT with streptavidin conjugated to FITC at a 1:200 dilution in blocking buffer. Cells were then washed 3x with PBS and mounted on slides with Prolong® Gold Antifade Mountant (ThermoFisher #P36935) and left to dry overnight in the dark at RT. Images were acquired with a Leica SP-8 confocal microscope. For quantifications, biological triplicates of each condition were analyzed by generating 3x3 tiles at 40x objective three times from each slide.

Western blot analysis. Bafilomycin A (Sigma, #B1793) treatment was at 20nM for 6 hours. Cycloheximide (Sigma #C104450) treatment was at 200µg/ml and cells lysed at 6, 12, or 24 hours after addition. For p53 stabilization, cells were exposed to 25 Gy ionizing radiation and lysed 4 hours later. SDS/PAGE gels were run under reducing conditions and immunoblotted on nitrocellulose membranes. 25µg of protein was run on 12% acrylamide gels for detection of HA (Sigma #H3663), uS12 (Santa Cruz #sc-100837), uL5 (RPL11) (Abcam #ab79352), tubulin (Sigma #T6199), and LC3 (Abcam #ab51520). 10% acrylamide gels were run for detection of p53 (Santa Cruz, #sc-6243) and phospho-S6 kinase (Cell Signaling #92345). 4-20% acrylamide gels were used for the cycloheximide experiments. Primary antibodies were diluted 1:1000 in 5% milk in TBST and incubated overnight at 4°C. For detection of p53, pS6k, and LC3HRP-conjugated secondary antibodies were diluted 1:10,000 at RT for one hour and detected with ECL reagents (Amersham) and exposed to film. For detection of uS12, HA, uL5, and tubulin the Odyssey detection kit (LI-COR) was used. Quantifications were performed with ImageJ software.

Sucrose cushion experiment. Transfected HEK293 cells were lysed in polysomal lysis buffer (supplemented with 110mM potassium acetate, 20mM magnesium acetate, 10mM HEPES, 100mM potassium chloride, 10mM magnesium chloride, 0.1% NP-40, 2mM DTT, 40U/mL RNase inhibitor [Thermo Fisher #10777019), 100ug/ml cycloheximide [Sigma #C104450] and 1X Protease inhibitor Cocktail V [Calbiochem]). Lysates were treated with 1500 U RNAse1 (Ambion) for 30 min at 21° C and loaded onto 6 ml polysome lysis buffer layered over 4 ml 32% sucrose cushions. Tubes were centrifuged in a SW41 rotor for 2.5h in a Beckman Coulter L-100 XP ultracentrifuge. The supernatants were removed and pellets were dissolved in 6x SDS loading buffer for western blot analysis.

Results

A missense mutation is identified in *RPS23* at c.200G>A in an individual with ID, ASD, and hearing loss. Trio exome sequencing identified a *de novo* Chr5(GRCh37):g.81572302C>T; NM_001025.4:c.200G>A (p.[Arg67Lys]) mutation in the *RPS23* gene of a 10-year old male that was absent in both parents. Sanger sequencing confirmed the mutation in fibroblasts (Figure S1A). Queries in BioMuta, DMDM, the NHLBI Exome database, and NCBI did not reveal any previously reported SNPs corresponding to Arg67. The individual presents with a mild ID, ASD, and hearing loss. Additionally the individual has a broad range of dysmorphic features often associated with ID/ASD such as simian palmar creases, epicanthic folds in the eyes, fetal finger pads, extra front teeth, low back hairline, facial asymmetry, and high palate (Table 1)[28; 29]. Hypotonia at birth was also noted. No abnormal hematology results were found by routine analysis (Table 2). A case report shows the individual's brittle hair has structural abnormalities compared to family members[30].

A variant in yeast uS12 orthologous to p.Arg67Lys affects growth of a unicellular eukaryote. The affected Arg67 lies in a loop region of uS12, PNSA, which is completely conserved in all three domains of life (Figure S1B)[10]. The PNSA loop interacts with aminoacyl-tRNAs, 18S rRNA, and the decoding center of the ribosome upon binding of a cognate anticodon-stem-loop[31]. Substitution of amino acids within this loop alters translational accuracy, including Lys42 in *E. coli* and Lys62 in *S. cerevisiae* (both analogous to Lys60 in humans)[10-12]. Because of the clear importance of the PNSA loop in ribosome function, the affected human Arg67 was examined at the atomic level. Structural analysis of uS12 from a cryo-EM reconstruction of the human 80S ribosome revealed the position of Arg67 and its predicted polar contacts (hydrogen bonds). Two polar contacts occur between Arg67 and guanosine 617 in the 18S rRNA (Figure 1A). Other polar contacts occur internally with Asp114

in uS12 (Figure 1A)[24]. In addition, Arg67 is closely situated in proximity to a prolyl residue (Pro62) in uS12 that, like Asp114, is completely conserved (Figures 1A and S1A). Substitution of the arginine at position 67 in uS12 with a lysine is predicted by PyMOL to abolish the polar contacts normally maintained by Arg67 with guanosine 617 in the 18S rRNA (Figure 1B).

To investigate the cellular consequences of the uS12 p.Arg67Lys variant, its effects were tested in *S. cerevisiae*. Haploid yeast cells contain two *RPS23* orthologues, presently named *RPS23A* and *RPS23B*, which encode identical uS12 proteins. A strain was constructed to test the effects of the mutant form of uS12 as the sole form of uS12 protein in cells. This strain was constructed harboring a complete deletion of *RPS23B* (*rps23b*Δ*::HIS3MX6*) in which *RPS23A* transcription was under the control of the glucose-repressible, galactose-inducible *GAL4* promoter (*GAL::RPS23A).* Episomal high copy vectors were also constructed enabling constitutive heterologous expression of the wild-type and variant forms of uS12 (Figure 1C). Both the endogenous uS12 and plasmid-borne uS12 are produced in medium containing galactose and lacking glucose, but only plasmid-borne uS12 is produced in media containing glucose and lacking galactose. Depletion of endogenous uS12 was confirmed by western blotting (Figure 1D, lane 2). The levels of uS12 from the plasmid (Figure 1D; lane 4, 6, 8, 10, 12) are at or above the level for undepleted EV (Figure 1D, lane 1), which represents only endogenous levels of uS12 (Rps23) protein. Therefore, all variant uS12 proteins are found near the levels of the endogenous protein in this system.

Site-directed substitutions in the plasmid-expressed uS12 were generated including p.Arg69Lys, p.Arg69Glu, p.Arg69His, and p.Lys62Arg. p.Arg69Lys is orthologous to the human uS12 p.Arg67Lys substitution (see alignment in Figure S1B). p.Arg69Glu and p.Arg69His were employed to test the effect of amino acid charge at that same residue, whilst the p.Lys62Arg substitution (previously shown to negatively affect translational fidelity in yeast) served as a control[11]. Serial dilutions were spotted onto plates containing galactose or glucose of the *GAL::RPS23A rps23b*Δ strain transformed with the p424GPD plasmids. In galactose (Figure 1E, left panels, 3 and 7 days of growth), no differences among the

substitutions can be seen, indicating even spotting of the yeast cultures and no dominant negative effects of the substitutions. In glucose (Figure 1E, right panel), plasmid-borne wild-type uS12 was able to rescue growth defects caused by depletion of endogenous uS12 (Figure 1E, right panel, compare EV vs. WT at 3 days of growth). However, uS12 p.Arg69Lys did not rescue growth to the same degree as wild-type uS12 (Figure 1E, right panel, 3 days of growth), indicating that p.Arg69Lys is a deleterious variant. The colony size of the yeast producing uS12 p.Arg69Lys is also smaller, indicating impaired growth (Figure 1E, right panel, 3 and 7 days of growth). Interestingly, the known deleterious uS12 p.Arg69Lys variant rescued growth to a comparable degree as uS12 p.Lys62Arg (Figure 1E, right panel, 3 days of growth). In contrast, replacement of the positively charged arginine at position 69 with a negatively charged glutamate was not able to rescue growth. Moreover, substitution to histidine (a positively charged amino acid like arginine and lysine) at position 69 in uS12 was able to rescue growth of yeast when grown to saturation (Figure 1E, right panel, 7 days of growth), albeit to a lesser degree than the p.Arg69Lys substitution. Taken together, these results highlight the importance of a positively charged amino acid at position 69 in uS12. Nevertheless, as neither the p.Arg69Lys or p.Arg69His variants were able to rescue growth to the same degree as wild-type uS12, the importance of Arg69 cannot simply lie in its positively charged side chain. These results support the hypothesis that the p.Arg67Lys missense substitution results in a human uS12 that is likely only partially functional, and thus could be a pathogenic hypomorphic allele.

The uS12 p.Arg67Lys variant affects ribosome biogenesis but not cell proliferation, *de novo* protein synthesis rates, or the ribosomal stress response. To investigate the functional consequences of uS12 p.Arg67Lys on ribosome biogenesis, EBV-immortalized lymphoblast cell lines (LCLs) were compared to a knockdown of uS12. The knockdown of many RPs, including uS12, results in accumulation of pre-rRNA molecules early in the processing pathway[32; 33]. In recapitulation, uS12 in HeLa cells was knocked down to analyze

accumulations of pre-rRNA by RAMP (ratio analysis of multiple precursors)[34]. Reductions in free 40S subunits by polysome profiling analysis confirmed the efficacy of the knockdown (Figure S2A). An accumulation of 30S pre-rRNA was revealed by northern blotting with ITS1 (internally transcribed spacer-1) probes alongside a reduction of 21S and 18S-E (Figure 2A,B). Analysis of the effect of the uS12 p.Arg67Lys substitution in the LCL, however, suggested a different and much later defect in pre-rRNA processing. Northern blot analysis revealed an accumulation of 18S-E pre-rRNA in uS12 p.Arg67Lys cells, suggesting one of the final steps of pre-rRNA maturation is impaired (Figures 2A,B). Probes against ITS2 and ITS1-5.8S did not reveal any major differences in cells with knocked down uS12 or carrying the p. Arg67Lys variant (Figure S2B). Included in the analysis is an LCL derived from an individual with DBA carrying a mutation in the *RPS24* gene, which codes for eS24 (RPS24). These cells revealed the expected early processing defect evident by 30S pre-rRNA accumulation (Figures 2A,B). A full schematic of mammalian pre-rRNA processing is shown in Figure S2C and a highlight of the relevant portion of the pathway is shown in Figure 2C[33].

Polysome profiles of LCL extracts derived from a healthy control individual revealed the expected ratio of small 40S to large 60S ribosomal subunits (Figure 2D,F). In contrast, the number of mature 40S subunits was reduced in cells carrying the uS12 p.Arg67Lys substitution (Figure 2 E,F). Western blot analysis showed that this reduction of 40S subunits was not due to a reduction of total uS12 protein in the cells (Figure S2D,E) and RNA sequencing of polyA-RNAs isolated from LCLs showed there was equal expression of wild-type and mutant alleles transcribing *RPS23* mRNAs (Figure 2G).

Further analysis revealed that while LCLs derived from an individual with DBA displayed reduced cell proliferation compared to two unrelated healthy controls, proliferation of the uS12 p.Arg67Lys LCL was unaffected (Figure 2H). Similarly, *de novo* protein synthesis, as determined by fluorescence-based AHA incorporation, was reduced in the DBA LCL but remained unchanged in the uS12 p.Arg67Lys LCL (Figure 2I).

DBA-linked RP haploinsufficiency causes a number of ribosomal stress responses including autophagy, S6 kinase phosphorylation, and/or stabilization of the p53 tumor suppressor[35; 36]. Western blotting of cells carrying the uS12 variant did not reveal any changes in the ratio of LC3-I to LC3-II proteins, a measurement indicative of autophagy (Figure S3A)[37]. No increase in S6K phosphorylation or changes in p53 stabilization were observed in uS12 p.Arg67Lys cells compared to healthy control cells (Figure S3B,C). These results together suggest that the ID and dysmorphism in the uS12 individual are due to a ribosomal dysfunction that does not manifest as a reduction of protein synthesis or in the subsequent ribosome stress response.

A second variant linked to dysmorphism destabilizes uS12. Having established that the p.Arg67Lys variant is likely pathogenic but does not cause a DBA-like phenotype, additional evidence was sought to link uS12 to syndromic phenotypes. A 5-year old female was identified with a *de novo* mutation in *RPS23* at Chr5(GRCh37):g.81005179>A; NM_001025.4:c.358T>A (p.[Phe120Ile]). Trio exome sequencing confirmed neither parent carried the mutation. Sanger sequencing confirmed the mutation in fibroblasts (Figure S1A). Queries in BioMuta, DMDM, the NHLBI Exome database, and NCBI did not reveal any previously reported SNPs corresponding to Phe120. The affected phenylalanine lies in another highly conserved loop region of uS12, PGVRY (Figure S1B). This aromatic residue is invariant in Eukarya and strongly conserved in Archaea and Bacteria, where the residue is an aromatic tyrosine (Figure S1B). The PGVRY loop region of uS12, similar to PNSA, makes contact with the decoding center of the ribosome and is also the site of substitutions that affect translational fidelity in *E. coli* and reduce growth in *S. cerevisiae*[10; 11]. The individual with the uS12 p.Phe120Ile variant, similar to the p.Arg67Lys individual, presented with hearing loss and many similar dysmorphisms such as microcephaly, short stature, epicanthic eye folds, low back hairline, low set ears, palmar creases, short fifth digits, and fetal finger pads (Table 1). The p.Phe120Ile individual also presented with submuccous cleft palate, a bifid uvula, and Raynaud-like

phenomena in response to cold. In contrast to the p.Arg67Lys indivivdual, the p.Phe120Ile individual has no intellectual disability and is communicative (Table 1). The cryo-EM structure of the 80S ribosome revealed that the Phe120 residue is predicted to interact with Phe41 in uS12 through pi-pi stacking (Figure 3A)[24]. Substitution of Phe120 with a non-aromatic isoleucine would abolish pi-pi stacking and potentially result in a structural change that affects the stability of uS12 (Figure 3B).

To determine the extent of the predicted effect of the substitutions on uS12 stability, protein levels of uS12 were measured in human dermal fibroblasts. Untreated wild-type and mutant fibroblasts revealed equivalent levels of uS12 (Figure 3C,D). However, when *de novo* protein synthesis was blocked with cycloheximide, a reduction of uS12 protein was detected over time in cells carrying the p.Phe120Ile variant but not in healthy control cells (Figures 3C,D). We did not observe significant destabilization of uS12 in p.Arg67Lys fibroblasts treated with cycloheximide (data not shown).

To determine if the substitutions affect the ability of uS12 to assemble into ribosomal complexes, plasmids expressing wild-type and mutant HA-tagged uS12 were transfected into HEK293 cells. In whole cell lysates, a lesser amount of HA-uS12 p.Phe120Ile protein was evident compared to equivalent levels of HA-uS12 wild-type and HA-uS12 p.Arg67Lys protein (Figure 3E,F). Cell lysates were then size-separated by ultracentrifugation on a 32% sucrose cushion. Both HA-uS12 wild-type and HA-uS12 p.Arg67Lys were detected in the high-density pellets that were devoid of tubulin but enriched with uL5 (RPL11) (Figure 3E,F). In contrast, far less HA-tagged protein was detected in the pellets of cells transfected with plasmids encoding HA-uS12 p.Phe120Ile (Figure 3E,F). This suggests the destabilizing effect of the p.Phe120Ile substitution in uS12 may be impairing the involvement of the variant in pre-40S biogenesis at an earlier point in subunit formation than the p.Arg67Lys substitution.

Polysome profiling of fibroblasts revealed different abnormalities compared to healthy control cells (Figures 3G-I). Compared to the clear reduction of 40S subunits in LCLs with the uS12

p.Arg67Lys variant (Figures 2E,F), the variant in fibroblasts instead has a much more pronounced effect on the 80S monosome (Figures 3H,J). In contrast, the profiles of fibroblasts carrying the p.Phe120Ile substitution do reveal a significant reduction of 40S subunits in addition to fewer 80S monosomes (Figures 3I,J). It is possible that this discrepancy is due to the much faster rate of LCL proliferation compared to fibroblasts. This is evident when comparing the size of the polysome peaks, which are robust in LCLs (Figures 2D,E) and undetectable in fibroblasts (Figures 3G-I). This greater demand for ribosome biogenesis in LCLs may result in an amplification of detectable differences in subunit amounts, and unfortunately LCLs from the individual with the p.Phe120Ile variant were not available to fully test this. However, the polysome profiling of fibroblasts from both individuals reveal reductions of monosomes, and add further evidence that the uS12 p.Phe120Ile variant may have a greater effect on pre-40S subunit formation than the p.Arg67Lys variant.

Quantitative RT-PCR was then used to determine if the expression of uS12 mRNA is compensating for defective uS12 protein in fibroblasts carrying the variant. When expressed relative to βactin mRNA, a striking increase in uS12 mRNA was noted in the variant fibroblasts compared to healthy control cells (Figure 3K). This may reflect an attempt by the cells carrying the variants to ramp up synthesis of wild-type alleles coding for uS12 as a response to the apparent difficulties in generating functional ribosomes for active translation.

p.Arg67Lys impairs uS12 hydroxylation by OGFOD1. The conserved prolyl residue at codon 62 in human uS12 is hydroxylated by the 2-OG oxygenase OGFOD1[13]. OGFOD1 forms discrete associations with uS12 that can be visualized as differentially migrating species in SDS-PAGE[13]. Hydroxylation of uS12 leads to the formation of a high-affinity protein complex with OGFOD1 that migrates as an ~100 kDa adduct by SDS-PAGE. This association is separable from a lower-affinity interaction that is hydroxylation-independent and is reducible by denaturing electrophoresis. Using the presence of the 100 kDa adduct as a surrogate for uS12 hydroxylation, parallel OGFOD1 immunoprecipitations were performed in LCLs derived from a healthy control or the individual carrying the uS12 p.Arg67Lys variant. Equivalent

capture of uncomplexed OGFOD1 (~75 kDa) was observed in both p.Arg67Lys and control lysates. However, capture of the ~100 kDa hydroxylation-dependent species was significantly reduced in p.Arg67Lys lysate compared to healthy control lysate (Figure 4A; lane 3, 6). This was in the absence of any effect on uS12 binding at its native molecular weight, as determined by uS12 immunoblotting (Figure 4A).

LCLs were not available from the individual carrying the p.Phe120Ile variant. To assay the effect of the p.Phe120Ile substitution on uS12 binding to OGFOD1, plasmids coding for HA-tagged uS12 were transiently co-expressed with those coding for FLAG-OGFOD1 in HEK293 cells and anti-HA (uS12) pulldowns were performed. Concordant with endogenous IPs, HA-uS12 p.Arg67Lys co-purified FLAG-OGFOD1 but did not form the 100 kDa adduct (Figure 4B). In contrast, high-affinity HA-uS12 p.Phe120Ile:FLAG-OGFOD1 complexes were detected, albeit to a lesser degree than wild-type uS12 due to lower protein levels of uS12 p.Phe120Ile (Figure 4B). These data suggest that the p.Arg67Lys substitution impairs uS12 hydroxylation by OGFOD1 without affecting protein:protein interaction, and that destabilized uS12 p.Phe120Ile likely results in fewer hydroxylated uS12 proteins.

To directly assay the effect of the p.Arg67Lys substitution on hydroxylation and incorporation of uS12 into the ribosome we isolated endogenous uS12 from polysomes derived from healthy control and p.Arg67Lys LCLs by sucrose density ultracentrifugation and reverse phase chromatography. uS12 was subjected to proteolytic digestion with trypsin and peptides were analyzed by liquid chromatography tandem mass spectrometry (LC-MS/MS). The relative abundance of the mutant peptide was monitored in ribosomes derived from the p.Arg67Lys LCL by measuring peak intensities of equivalent wild-type and p.Arg67Lys precursor ions assigned by MS/MS (Table S1). Ion intensities of wild-type and p.Arg67Lys peptides were summed and expressed as a relative ratio. Quantifying data from 5 independent experiments indicated a marked reduction of p.Arg67Lys peptides in polysomal ribosomes with less than 10% of the total peptide counts carrying the p.Arg67Lys substitution (Figure 4C). As no decrease in polysome size or suppression of mutant allele expression in the LCL was detected

(Figure 2C-F), this suggests that a mechanism exists preventing ribosomes carrying the uS12 variant from entering the polysomal pool.

We next considered the effect of the substitution on OGFOD1-dependent catalysis, seeking to corroborate interaction data with direct measurement of hydroxylation by mass spectrometry. Fortuitously, the p.Arg67Lys substitution preserves a trypsin cleavage site and is present on all peptides that contain the target prolyl hydroxylation site. This enabled direct measurement of the effect of the p.Arg67Lys substitution on uS12 hydroxylation at the peptide level in ribosomes isolated from LCLs.

Relative quantitation indicated a deleterious effect of the p.Arg67Lys substitution on Pro62 hydroxylation with <40% of the Lys67-bearing peptides recovered from ribosomes hydroxylated. (Figure 4D, Figure S4 for representative extracted ion chromatograms and MS/MS assignments and Table S1 for Summary). In contrast, wild-type uS12 peptides with Arg67 extracted from the same cells, and from separate healthy control LCLs, were near fully hydroxylated (>95%; Figure 4D). High levels of wild-type uS12 hydroxylation in LCLs carrying p.Arg67Lys uS12 argue against the substitution having a significant dominant negative function in this context. These results show that the substitution of lysine for arginine at amino acid position 67 has detrimental consequences for hydroxylation of uS12 by OGFOD1, and that very few ribosomes carrying the variant protein are incorporated into the polysomal pool.

uS12 variants intensify stress granule formation and affect translational fidelity. Cellular stress such as hypoxia or heat shock induces the formation of cytoplasmic stress granules as a mechanism to suppress the translation of mRNAs not immediately required for the stress response[38]. Stalled pre-initiation complexes that include 40S subunits and small RPs are rapidly sequestered in stress granules upon assembly by the GTPase-activating protein SH3 domain binding protein 1 (G3BP1)[39]. Deregulated stress granule formation is being revealed as an important indicator of several human pathologies, including neuronal dysfunction and

degeneration[40]. Because acute loss of OGFOD1 drives G3BP1+ stress granule formation in U2OS cells[13], their formation in the uS12 variant cells was investigated.

Fibroblasts derived from healthy controls and the individuals carrying uS12 variants were exposed to arsenite to induce oxidative stress. Stress granules in these cells were then stained by immunofluorescence and analyzed by confocal microscopy. In all cell types, G3BP1 localized diffusely throughout the cytoplasm and aggregated in granules of about 100-200 nm in size when treated for 30 minutes with 500 µM arsenite (Figure 5A). However, the percentage of cells revealing stress granules when exposed to increasing concentrations of arsenite was consistently higher in cells carrying either the uS12 p.Arg67Lys or p.Phe120Ile substitution compared to healthy control cells (Figures 5A,B and S5). These data suggest that the uS12 variants affect the dynamics of stress granule formation, and render cells particularly sensitive to oxidative stress.

Increased oxidative stress levels or reduced levels of OGFOD1 change the fidelity of protein translation[13; 41]. This can manifest as changes in suppression of missense mutations, readthrough of stop codons, or in rates of -1 or +1 Programmed Ribosomal Frameshifting (-/+1 PRF) on so-called “slippery sites”, and can be measured with dual luciferase reporter plasmids (Figure S6)[23].

The uS12 p.Arg69Lys (Arg67 in humans) substitution had a pronounced effect on translational fidelity in yeast. Experiments were performed alongside a strain carrying p.Lys62Arg substitution that has been previously reported to affect translational fidelity[11; 12]. Similar to the uS12 p.Lys62Arg variant, the strain carrying the p.Arg69Lys variant displayed altered rates of -1 PRF in a sequence-dependent manner (Figure 5C). Additionally, uS12 p.Arg69Lys increased the rate at which ribosomes read through UAA and UAG stop codons (Figure 5D). The p.Arg218Ser substitution when introduced into the firefly protein renders the luciferase inactive[20]. However, when this substitution is introduced with a non-cognate DNA mutation (AGA [arginine]->TGT [serine]) yeast cells carrying the uS12 p.Arg69Lys variant were more

likely to select the missense arginine residue instead of the serine (Figure 5E). No changes in EST3-directed +1 PRF as a result of uS12 p.Arg69Lys were detected (Figure 5F). +1 PRF is entirely driven by interactions between the peptidyl-tRNA, the ribosomal P-site, and the mRNA. In contrast, -1 PRF involves both the P- and A-sites, while near- and non-cognate tRNA interactions involve the ribosomal A-site[42]. By process of elimination, it is likely that the uS12 variants are affecting A-site but not P-site function.

Translational fidelity was also assayed in the human fibroblasts. Cells carrying uS12 p.Arg67Lys or p.Phe120Ile revealed a significant increase in the rate of UAA stop codon readthrough compared to healthy control cells (Figure 5G). Together, these results suggest that the human uS12 variants, similar to what was reported previously in *E. coli* [10-12], adversely affect the decoding of mRNA and the fidelity of protein translation.

Discussion

This study suggests that uS12 variants affecting the ability of ribosomes to correctly decode mRNA drive human dysmorphism and in some cases can also impair neurodevelopment. Comparable developmental defects were presented in unrelated individuals with missense substitutions in two highly conserved loop regions of uS12 that in bacteria and yeast are important for translational accuracy and growth[10-12]. The p.Phe120Ile substitution destabilized the uS12 protein and the p.Arg67Lys substitution impaired OGFOD1 hydroxylation, an event known to be important for translational fidelity[13]. Despite a mild ribosome biogenesis defect in LCLs carrying the p.Arg67Lys substitution, there was no indication of proliferation impairment or changes in the rate of protein synthesis as is commonly observed in LCLs derived from individuals with DBA. However, ribosomes carrying uS12 variants were less able to accurately decode mRNA codons. This is readily apparent in the yeast model, where the only form of uS12 is the variant. Of course this is different in diploid human cells where both wild-type and mutant copies of *RPS23* are expressed, thus the human mutations are haploinsufficient as is the case with many other ribosomopathies such as DBA. This underscores the centrality of a functioning ribosome and shows how even small changes can be greatly amplified in complex developmental processes.

The scarcity of uS12 peptides with Lys67 in the polysomal pool of LCLs is particularly interesting in light of the equal expression in these cells of both wild-type and mutant alleles. uS12 p.Arg67Lys does not appear to impair 40S assembly until very late stages (as in LCLs) if at all (as in fibroblasts), suggesting the existence of a quality control mechanism that identifies 40S subunits with the uS12 variant and largely prevents them from entering the polysomal pool. One possibility is that the uS12 variant is being replaced with a wild-type uS12. This process of ribosome repair by replacing damaged RPs, specifically uS12, has been previously described in *E. coli*[43]. A similar mechanism might occur in the human context, where ribosomes carrying an unhydroxylated, unstable, or absent uS12 are held in stalled pre-initiation complexes while a repair is made. Since pre-initiation complexes are coordinately

recruited to stress granules in response to oxidative stress[44], this may explain the more rapid formation of these structures in the fibroblasts carrying the uS12 variants upon exposure to arsenite.

These results may also shed light on the question of why RP gene mutations affect such discrete tissue types. All cells in the body express all the RPs, albeit not necessarily equally, and it has been a puzzle as to why the haploinsufficient loss of specific RP genes results in such tissue-specific effects. Perhaps the answer lies in how much of the wild-type RP gene is expressed and available in a particular cell type or subcellular location for ribosome repair. To use ICA as an example, individuals with *RPSA* mutations suffer severely impaired development of the spleen but no hematopoietic (or any other major) phenotype. Conversely, asplenia is not reported in individuals with DBA. Tagged uS2 proteins carrying substitutions linked to ICA are, like the uS12 p.Phe120Ile variant reported here, unstable and levels are so low as to be undetectable in some cases[3]. However these variants, like uS12 p.Arg67Lys, do not seem to adversely affect LCLs in contrast to DBA-linked RP variants[3]. Thus the ability to compensate for lost or defective RPs seems to depend on which RP is impaired in which cell type. Extending this analysis to DBA, if erythrocyte progenitor cells express less of the wild-type allele to replace the RP variant in comparison to other hematopoietic cell types, this may explain the pure red cell aplasia. If the wild-type RP allele expression in erythrocyte progenitors varies between individuals, this may be why some healthy parents can carry a mutant RP gene (or “silent mutation”) that is pathogenic in their offspring. As the number of human disorders linked to RP gene mutation continues to increase, further studies into the reasons underlying tissue-specific defects are definitely warranted.

This study reveals the pathogenicity of a previously undescribed ribosomopathy and suggests that while the hematopoietic phenotypes resulting from RP gene mutations are largely due to reductions in mRNA translation rates, these mutations reported in *RPS23* instead drive developmental disorders by coding for uS12 variants that impair the ability of ribosomes to accurately decode mRNA. The implications of this may well go beyond RP gene mutations.

Translational fidelity defects, such as increased rates of frameshifting, have been reported in yeast carrying a mutation in the sister chromatid cohesion 2 gene (*SCC2*)[45]. This mutation impairs rRNA production and ribosome assembly but does not affect protein synthesis rates[45]. Orthologous mutations of this gene, Nipped-B (*NIPBL*), are found in individuals with Cornelia de Lange syndrome (OMIM #122470). Individuals with this syndrome feature many of the same clinical phenotypes as the individuals reported here, including the ID/ASD, hearing loss, microcephaly, hypotonia at birth and delayed motor development, abnormal hair growth (such as long eyelashes and bushy eyebrows with synophrys), low set ears, the palmar crease, and short fifth digits. Thus translational inaccuracy may be an underlying cause of developmental defects in a much wider spectrum of human disorders than is currently appreciated.

Acknowledgements

Very special thanks go to all the individuals in this study and their families. We thank Prof. Hans Brunner of the Radboud University Nijmegen Medical Centre and Prof. Nine Knoers of the University Medical Center Utrecht for performing the exam sequencing as well as Daisy Picavet and the AMC Cellular Imaging Core Facility for assistance with the confocal microscopy. Mass spectrometry analysis was performed in the TDI MS laboratory led by Benedict M. Kessler. AM, AA, MW, PEG, and MOD are supported under the frame of E-Rare-2, ERA-Net for Research on Rare Diseases (ZonMW #113301205 and #40-44000-98-1008 in the Netherlands, #BMBF 01GM1301 in Germany, #ANR-15-RAR3-0007-04 in France). The Landsteiner Foundation supported NP and FS for Blood Transfusion Research (#1239). CV was supported by the National Institutes of Health (NIH) / National Heart Lung Blood Institute (R01HL119439 to JD). SB was supported by NIH / General Medical Sciences (R01GM115710). SS was supported by National Institutes of Health (NIH) / Diabetes and Digestive and Kidney Diseases / General Medical Sciences / Child Health and Human Development (F30DK109582, T32GM07205, and T32HD007149 to SS). The Ludwig Institute of Cancer Research supported MA, MC and PR. PG and MO were supported by the Agence National de la Recherche, (project DBA-Multigenes).

References

1. Boria, I., Garelli, E., Gazda, H.T., Aspesi, A., Quarello, P., Pavesi, E., Ferrante, D., Meerpohl, J.J., Kartal, M., Da Costa, L., et al. (2010). The ribosomal basis of Diamond-Blackfan Anemia: mutation and database update. Human mutation 31, 1269-1279.
2. Ebert, B.L., Pretz, J., Bosco, J., Chang, C.Y., Tamayo, P., Galili, N., Raza, A., Root, D.E., Attar, E., Ellis, S.R., et al. (2008). Identification of RPS14 as a 5q- syndrome gene by RNA interference screen. Nature 451, 335-339.
3. Bolze, A., Mahlaoui, N., Byun, M., Turner, B., Trede, N., Ellis, S.R., Abhyankar, A., Itan, Y., Patin, E., Brebner, S., et al. (2013). Ribosomal protein SA haploinsufficiency in humans with isolated congenital asplenia. Science 340, 976-978.
4. Brooks, S.S., Wall, A.L., Golzio, C., Reid, D.W., Kondyles, A., Willer, J.R., Botti, C., Nicchitta, C.V., Katsanis, N., and Davis, E.E. (2014). A novel ribosomopathy caused by dysfunction of RPL10 disrupts neurodevelopment and causes X-linked microcephaly in humans. Genetics 198, 723-733.
5. Thevenon, J., Michot, C., Bole, C., Nitschke, P., Nizon, M., Faivre, L., Munnich, A., Lyonnet, S., Bonnefont, J.P., Portes, V.D., et al. (2015). RPL10 mutation segregating in a family with X-linked syndromic Intellectual Disability. American journal of medical genetics Part A 167A, 1908-1912.
6. Zanni, G., Kalscheuer, V.M., Friedrich, A., Barresi, S., Alfieri, P., Di Capua, M., Haas, S.A., Piccini, G., Karl, T., Klauck, S.M., et al. (2015). A Novel Mutation in RPL10 (Ribosomal Protein L10) Causes X-Linked Intellectual Disability, Cerebellar Hypoplasia, and Spondylo-Epiphyseal Dysplasia. Human mutation 36, 1155-1158.
7. Vlachos, A., Ball, S., Dahl, N., Alter, B.P., Sheth, S., Ramenghi, U., Meerpohl, J., Karlsson, S., Liu, J.M., Leblanc, T., et al. (2008). Diagnosing and treating Diamond Blackfan anaemia: results of an international clinical consensus conference. British journal of haematology 142, 859-876.
8. De Keersmaecker, K., Atak, Z.K., Li, N., Vicente, C., Patchett, S., Girardi, T., Gianfelici, V., Geerdens, E., Clappier, E., Porcu, M., et al. (2012). Exome sequencing identifies mutation in CNOT3 and ribosomal genes RPL5 and RPL10 in T-cell acute lymphoblastic leukemia. Nat Genet.
9. Stark, H., Rodnina, M.V., Wieden, H.J., Zemlin, F., Wintermeyer, W., and van Heel, M. (2002). Ribosome interactions of aminoacyl-tRNA and elongation factor Tu in the codon-recognition complex. Nature structural biology 9, 849-854.
10. Sharma, D., Cukras, A.R., Rogers, E.J., Southworth, D.R., and Green, R. (2007). Mutational analysis of S12 protein and implications for the accuracy of decoding by the ribosome. Journal of molecular biology 374, 1065-1076.
11. Anthony, R.A., and Liebman, S.W. (1995). Alterations in ribosomal protein RPS28 can diversely affect translational accuracy in Saccharomyces cerevisiae. Genetics 140, 1247-1258.
12. Synetos, D., Frantziou, C.P., and Alksne, L.E. (1996). Mutations in yeast ribosomal proteins S28 and S4 affect the accuracy of translation and alter the sensitivity of the ribosomes to paromomycin. Biochimica et biophysica acta 1309, 156-166.
13. Singleton, R.S., Liu-Yi, P., Formenti, F., Ge, W., Sekirnik, R., Fischer, R., Adam, J., Pollard, P.J., Wolf, A., Thalhammer, A., et al. (2014). OGFOD1 catalyzes prolyl hydroxylation of RPS23 and is involved in translation control and stress granule formation. Proceedings of the National Academy of Sciences of the United States of America 111, 4031-4036.
14. Hui-Yuen, J., McAllister, S., Koganti, S., Hill, E., and Bhaduri-McIntosh, S. (2011). Establishment of Epstein-Barr virus growth-transformed lymphoblastoid cell lines. Journal of visualized experiments : JoVE.
15. Longtine, M.S., McKenzie, A., 3rd, Demarini, D.J., Shah, N.G., Wach, A., Brachat, A., Philippsen, P., and Pringle, J.R. (1998). Additional modules for versatile and economical PCR-based gene deletion and modification in Saccharomyces cerevisiae. Yeast 14, 953-961.
16. Kushnirov, V.V. (2000). Rapid and reliable protein extraction from yeast. Yeast 16, 857-860.

17. Paganin-Gioanni, A., Bellard, E., Escoffre, J.M., Rols, M.P., Teissie, J., and Golzio, M. (2011). Direct visualization at the single-cell level of siRNA electrotransfer into cancer cells. Proceedings of the National Academy of Sciences of the United States of America 108, 10443-10447.
18. Ito, H., Fukuda, Y., Murata, K., and Kimura, A. (1983). Transformation of intact yeast cells treated with alkali cations. Journal of bacteriology 153, 163-168.
19. Advani, V.M., Belew, A.T., and Dinman, J.D. (2013). Yeast telomere maintenance is globally controlled by programmed ribosomal frameshifting and the nonsense-mediated mRNA decay pathway. Translation 1, e24418.
20. Plant, E.P., Nguyen, P., Russ, J.R., Pittman, Y.R., Nguyen, T., Quesinberry, J.T., Kinzy, T.G., and Dinman, J.D. (2007). Differentiating between near- and non-cognate codons in Saccharomyces cerevisiae. PloS one 2, e517.
21. Rakwalska, M., and Rospert, S. (2004). The ribosome-bound chaperones RAC and Ssb1/2p are required for accurate translation in Saccharomyces cerevisiae. Molecular and cellular biology 24, 9186-9197.
22. Harger, J.W., and Dinman, J.D. (2003). An in vivo dual-luciferase assay system for studying translational recoding in the yeast Saccharomyces cerevisiae. Rna 9, 1019-1024.
23. Jacobs, J.L., and Dinman, J.D. (2004). Systematic analysis of bicistronic reporter assay data. Nucleic acids research 32, e160.
24. Khatter, H., Myasnikov, A.G., Natchiar, S.K., and Klaholz, B.P. (2015). Structure of the human 80S ribosome. Nature 520, 640-645.
25. Sievers, F., Wilm, A., Dineen, D., Gibson, T.J., Karplus, K., Li, W., Lopez, R., McWilliam, H., Remmert, M., Soding, J., et al. (2011). Fast, scalable generation of high-quality protein multiple sequence alignments using Clustal Omega. Molecular systems biology 7, 539.
26. Cerami, E., Gao, J., Dogrusoz, U., Gross, B.E., Sumer, S.O., Aksoy, B.A., Jacobsen, A., Byrne, C.J., Heuer, M.L., Larsson, E., et al. (2012). The cBio cancer genomics portal: an open platform for exploring multidimensional cancer genomics data. Cancer discovery 2, 401-404.
27. Pereboom, T.C., van Weele, L.J., Bondt, A., and MacInnes, A.W. (2011). A zebrafish model of dyskeratosis congenita reveals hematopoietic stem cell formation failure resulting from ribosomal protein-mediated p53 stabilization. Blood 118, 5458-5465.
28. Taggart, L., and Cousins, W. (2014). Health Promotion For People With Intellectual And Developmental Disabilities.(Open University Press).
29. Ozgen, H., Hellemann, G.S., Stellato, R.K., Lahuis, B., van Daalen, E., Staal, W.G., Rozendal, M., Hennekam, R.C., Beemer, F.A., and van Engeland, H. (2011). Morphological features in children with autism spectrum disorders: a matched case-control study. Journal of autism and developmental disorders 41, 23-31.
30. Alsop, R.J., Soomro, A., Zhang, Y., Pieterse, M., Fatona, A., Dej, K., and Rheinstadter, M.C. (2016). Structural Abnormalities in the Hair of a Patient with a Novel Ribosomopathy. PloS one 11, e0149619.
31. Ogle, J.M., Brodersen, D.E., Clemons, W.M., Jr., Tarry, M.J., Carter, A.P., and Ramakrishnan, V. (2001). Recognition of cognate transfer RNA by the 30S ribosomal subunit. Science 292, 897-902.
32. Ferreira-Cerca, S., Poll, G., Gleizes, P.E., Tschochner, H., and Milkereit, P. (2005). Roles of eukaryotic ribosomal proteins in maturation and transport of pre-18S rRNA and ribosome function. Molecular cell 20, 263-275.
33. O'Donohue, M.F., Choesmel, V., Faubladier, M., Fichant, G., and Gleizes, P.E. (2010). Functional dichotomy of ribosomal proteins during the synthesis of mammalian 40S ribosomal subunits. The Journal of cell biology 190, 853-866.
34. Wang, M., Anikin, L., and Pestov, D.G. (2014). Two orthogonal cleavages separate subunit RNAs in mouse ribosome biogenesis. Nucleic acids research 42, 11180-11191.
35. Heijnen, H.F., van Wijk, R., Pereboom, T.C., Goos, Y.J., Seinen, C.W., van Oirschot, B.A., van Dooren, R., Gastou, M., Giles, R.H., van Solinge, W., et al. (2014). Ribosomal protein

mutations induce autophagy through S6 kinase inhibition of the insulin pathway. PLoS genetics 10, e1004371.
36. Pereboom, T.C., Bondt, A., Pallaki, P., Klasson, T.D., Goos, Y.J., Essers, P.B., Groot Koerkamp, M.J., Gazda, H.T., Holstege, F.C., Costa, L.D., et al. (2014). Translation of branched-chain aminotransferase-1 transcripts is impaired in cells haploinsufficient for ribosomal protein genes. Experimental hematology 42, 394-403 e394.
37. Feng, Y., He, D., Yao, Z., and Klionsky, D.J. (2014). The machinery of macroautophagy. Cell research 24, 24-41.
38. Arimoto, K., Fukuda, H., Imajoh-Ohmi, S., Saito, H., and Takekawa, M. (2008). Formation of stress granules inhibits apoptosis by suppressing stress-responsive MAPK pathways. Nature cell biology 10, 1324-1332.
39. Tourriere, H., Chebli, K., Zekri, L., Courselaud, B., Blanchard, J.M., Bertrand, E., and Tazi, J. (2003). The RasGAP-associated endoribonuclease G3BP assembles stress granules. The Journal of cell biology 160, 823-831.
40. Wolozin, B. (2014). Physiological protein aggregation run amuck: stress granules and the genesis of neurodegenerative disease. Discovery medicine 17, 47-52.
41. Netzer, N., Goodenbour, J.M., David, A., Dittmar, K.A., Jones, R.B., Schneider, J.R., Boone, D., Eves, E.M., Rosner, M.R., Gibbs, J.S., et al. (2009). Innate immune and chemically triggered oxidative stress modifies translational fidelity. Nature 462, 522-526.
42. Dinman, J.D. (2012). Mechanisms and implications of programmed translational frameshifting. Wiley interdisciplinary reviews RNA 3, 661-673.
43. Cukras, A.R., Southworth, D.R., Brunelle, J.L., Culver, G.M., and Green, R. (2003). Ribosomal proteins S12 and S13 function as control elements for translocation of the mRNA:tRNA complex. Molecular cell 12, 321-328.
44. Kedersha, N., Chen, S., Gilks, N., Li, W., Miller, I.J., Stahl, J., and Anderson, P. (2002). Evidence that ternary complex (eIF2-GTP-tRNA(i)(Met))-deficient preinitiation complexes are core constituents of mammalian stress granules. Molecular biology of the cell 13, 195-210.
45. Zakari, M., Trimble Ross, R., Peak, A., Blanchette, M., Seidel, C., and Gerton, J.L. (2015). The SMC Loader Scc2 Promotes ncRNA Biogenesis and Translational Fidelity. PLoS genetics 11, e1005308.

Figure Legends

Figure 1. Substitution of Arg69 in yeast uS12, orthologous to Arg67 in human uS12, results in growth defects. (A) Arg67 in wild-type uS12 is shown to be in close proximity with Pro62 with hydrogen bonds between 18S rRNA (left) that are not predicted to form with uS12 Lys67 **(B). (C)** Schematic of the yeast strains used for testing the effects of *RPS23* mutation in yeast uS12 on growth. In haploid yeast, one copy of *RPS23* was knocked out (*rps23b*Δ*::HIS3MX6*) and the other copy of *RPS23* was put under the control of a glucose-repressible, galactose inducible promoter (*GAL::RPS23A)*. **(D)** Immunoblotting with uS12 antibodies shows wild-type and mutated uS12 are found at the same levels from the p424GPD plasmid and endogenous uS12 is successfully depleted. U indicates undepleted endogenous uS12, and D indicates depleted endogenous uS12. EV indicates empty vector. **(E)** Substitutions of uS12 impairs growth of yeast on solid media. Serial dilutions of yeast expressing the indicated uS12 constructs were grown on solid media for the indicated number of days at 30ºC. Two biological replicates were performed starting with transformations of the plasmids into the yeast strain. EV indicates empty vector. See Figure S1 for multiple sequence alignment of uS12.

Figure 2. uS12 p.Arg67Lys affects ribosome biogenesis but not proliferation or *de novo* protein synthesis (A) Northern blot analysis of siRNA-treated HeLa cells or LCLs with 5'ITS1 probes. **(B)** RAMP analysis of 30S, 21S, and 18S-E alterations from (A) (N=3). **(C)** Polysome profiles of an LCL from a healthy individual. **(D)** Polysome profiles of the LCL from the uS12 p.Arg67Lys individual showing a reduction of 40S small ribosomal subunits (arrow). **(E)** Quantification of ratios of 40S:60S peak sizes from (C) and (D) (N=3). **(F)** RNA sequencing measurement of *RPS23* (uS12) wild-type and p.Arg67Lys alleles in LCLs. **(G)** Growth curves of LCLs over 5 days. The standard deviations for Healthy Control 1, Healthy Control 2, uS12 p.Arg67Lys, and DBA are as follows: Day 1 (+/-8.8e3, 2.7e4, 2.1e4, 9.5e3), Day 2 (+/-3.0e4, 1.5e4, 1.8e4, 1.7e4), Day 3 (+/-2.9e4, 3.8e4, 1.6e4, 1.7e4), Day 4 (+/-7.4e4, 6.9e4, 4.2e4,

2.2e4), and Day 5 (+/-8.5e4, 1.0e5, 6.0e4, 2.5e4). N=3. **(H)** *De novo* protein labeling measured over 30 minutes in LCLs from healthy controls, the individual with the uS12 p.Arg67Lys variant, or an individual with DBA. See also Figures S2 and S3. ***p*<0.01.

Figure 3. p.Phe120Ile affects stabilization of uS12 and 40S subunit levels while both p.Arg67Lys and p.Phe120Ile reduce 80S monosomes. (A) Phe120 in wild-type uS12 is in close proximity with Phe41 and likely creates pi-pi stacking which is absent with uS12 Ile120 (B)**. (C)** Western blot analysis of uS12 protein levels in healthy control and uS12 p.Phe120Ile variant fibroblasts subject to 200µg/ml cycloheximide (CHX) over 24 hours. **(D)** Quantification of protein levels in (C) (N=3) **(E)** Western blot analysis of HA-tagged protein levels in whole cell lysates of transfected HEK293 cells (lanes 1-4) or pellets resulting from lysates run over a 32% sucrose cushion. **(F)** Quantification of (E) (N=3). **(G-I)** Representative polysomes profiles of fibroblasts derived from healthy controls (G), the individual with the uS12 p.Arg67Lys variant (H), or the p.Phe120Ile variant (I). **(J)** Quantification and ratios of 40S, 60S, and 80S polysome peak sizes in (G-I). For controls N=8, for p.Arg67Lys N=3, for p.Phe120Ile N=4. Statistical analysis compares variant samples to healthy controls. **(K)** Quantitative real-time PCR results comparing the relative expression of uS12 to βactin cDNA transcribed from mRNA isolated from healthy or variant fibroblasts. N=3. **p*<0.05, ***p*<0.01, ****p*<0.001.

Figure 4. Substitutions perturb OGFOD1 binding and uS12 Pro62 hydroxylation. (A) Immunoprecipitation of endogenous OGFOD1 in LCLs from a healthy control individual or carrying the uS12 p.Arg67Lys variant immunoblotted with antibodies against OGFOD1 or uS12. The ~100 kDa high affinity complex is labeled (*). **(B)** Immunoprecipitation of ectopic HA-tagged uS12 variants in HEK293 cells co-expressing FLAG-OGFOD1. Anti-HA immunoprecipitates were immunoblotted with anti-HA and anti-FLAG antibodies to visualize uS12 and OGFOD1 respectively. The ~100 kDa high affinity complex is labeled (*). **(C)** Relative quantitation of wild-type and variant uS12 peptides in ribosomes isolated from

p.Arg67Lys LCLs. The abundance of endogenous uS12 tryptic peptides containing either Arg67 (wild-type) or Lys67 (mutant; p.Arg67Lys) was measured by mass spectrometry. Data (N=5) are presented as relative ratios of wild-type to p.Arg67Lys based on aggregate precursor ion intensities. **(D)** Pro62 hydroxylation level in ribosomes isolated from LCLs carrying the uS12 p.Arg67Lys variant compared to healthy control LCLs. Data are aggregate counts of precursor ions from independent biological replicates (healthy control, N=3; variant p.Arg67Lys, N=5) expressed as mean relative hydroxylation level +/- standard deviation. See Figure S4 for representative extracted ion chromatograms and Table S1 for peptide level counts. ****p*<0.001.

Figure 5. uS12 substitutions increase stress granules formation and impair translational fidelity. (A) Confocal microscopy of fibroblasts stained with G3BP1 antibodies either untreated (top) or treated with 500µM arsenite for 30 minutes (bottom). Note the formation of G3BP1+ stress granules in the arsenite treated cells. **(B)** Quantification of the percent of total fibroblasts from a healthy individual or the individuals carrying the uS12 variants that are stress granule positive upon treatment with increasing concentrations of arsenite for 30 min (N=3). The statistical analysis compares the variant cells to the healthy cells subject to similar treatment. See Figure S5 for representative images. **(C-F)** Translational fidelity assays in uS12 variant and wild-type yeast cells transformed with dual luciferase reporters described in Figure S6: **(C)** -1 PRF promoted by LA, EST1, EST2, or STN1 signals; **(D)** UAA or UAG readthrough; **(E)** Missense suppression with reporters carrying near- (AGA->AGC) or non-cognate (AGA->TGT) codons for R218; **(F)** +1 PRF with EST3 sequence. **(G)** UAA readthrough in primary fibroblasts from the individuals carrying the uS12 p.Arg67Lys or p.Phe120Ile variants and two unrelated healthy controls. See Figure S6 for luciferase reporter details. **p*<0.05, ***p*<0.01, ****p*<0.001.

	Individual 1 *RPS23* c.200G>A uS12 p.Arg67Lys	Individual 2 *RPS23* c.358T>A uS12 p.Phe120Ile
Face	Low nasal bridge Epicanthic folds Long eyelashes Blue sclerea Arched eyebrows, right eyebrow "different" Open mouth, thick under lip High arched palate	Low nasal bridge (as infant) Epicanthic folds Long eyelashes Bushy eyebrows with synophrys Submucous cleft palate and bifid uvula (corrected with surgery) Thin lips Periorbital fullness, round face as infant (as a baby face became less round)
Head	Small skull (-2.5 SD in infancy, -2.0 at age 12) Flat skull on backside Webbed neck as infant Right ear deformed and lower placed Two extra front teeth in upper jaw (surgically removed) Small lower jaw	Small skull (-2.5 SD at age 5) Flat skull on backside Right ear deformed and lower placed Mild low set ears, overlapping helix superior Normal teeth, permanent teeth more irregular placed than first teeth.
Skin/hair	Pigmented, elastic skin Hairy underarms Low back hairline Course skin on legs and arms Thin brittle hair	Normal, thick hair Hairy underarms/legs, is less prominent than as baby Low back hairline
Hands	Simian palmar crease Fetal fingerpads Short fifth finger Small brittle nails	Bilateral atypical simian palmar crease Fetal fingerpads Mild short fifth fingers Nails a bit broad, toe nails mildly concave.
Other	Loose joints/hypotonia as baby Hearing loss right ear Eye sight cylindric dev(r-3,5 l-2) Short stature at age 12 Disharmonic intellectual profile Non-verbal learning disability Right hip higher than left Autism Spectrum Disorder	Delayed motor development Bilateral conductive hearing loss (tubes, tonsils extirpated), now grossly normal hearing Normal vision Mild short stature Disharmonic intellectual profile Nonverbal>performal, intelligence in similar range as family members Raynaud-like phenomena in hands/feet when cold Is communicative

Table 1. Clinical features of individuals carrying *RPS23* gene mutations that code for uS12 variants.

	Individual 1 *RPS23* c.200G>A uS12 p.Arg67Lys	Individual 2 *RPS23* c.358T>A uS12 p.Phe120Ile
Hematology	Hemoglobin: 7.5 mmol/L MCV: 81.0 fL Leukocytes: 6.0 x 10.9/L Leukodifferentiation: Eosinophils: 3% Neutrophils: 64% Lymphocytes: 28% Monocytes: 6% Thrombocytes: 238 x 10.9/L	Hemoglobin: 8.0 mmol/L MCV: 81.0 fL Leukocytes: 7.9 x 10.9/L Leukodifferentiation: Eosinophils: 1% Neutrophils: 59% Lymphocytse: 33% Monocytes: 7% Thrombocytes: 183 x 10.9/L

Table 2. Hematology results from individuals carrying *RPS23* gene mutations that code for uS12 variants.

Figure 1

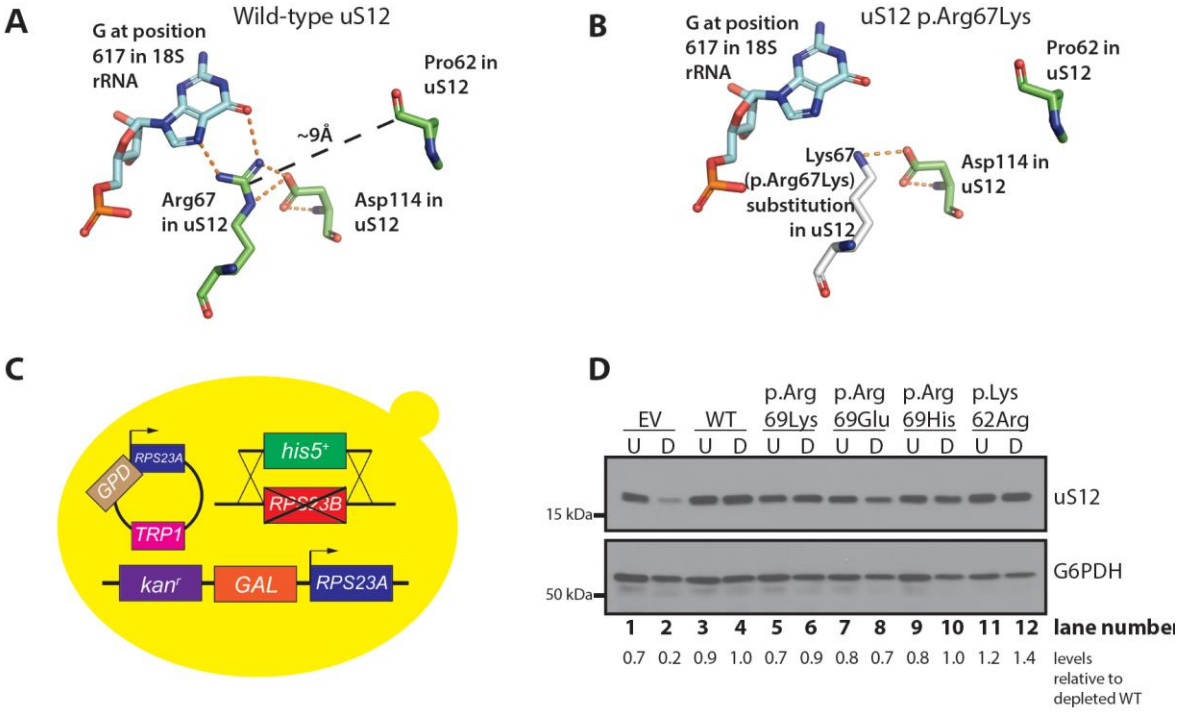
A
Wild-type uS12
G at position 617 in 18S rRNA
Pro62 in uS12
~9Å
Arg67 in uS12
Asp114 in uS12
B
uS12 p.Arg67Lys
G at position 617 in 18S rRNA
Pro62 in uS12
Lys67 (p.Arg67Lys) substitution in uS12
Asp114 in uS12
C
GPD
RPS23A
TRP1
his5+
RPS23B
kanr
GAL
RPS23A
D
EV
WT
p.Arg 69Lys
p.Arg 69Glu
p.Arg 69His
p.Lys 62Arg
U D U D U D U D U D U D
15 kDa
uS12
50 kDa
G6PDH
1 2 3 4 5 6 7 8 9 10 11 12
lane number
0.7 0.2 0.9 1.0 0.7 0.9 0.8 0.7 0.8 1.0 1.2 1.4
levels relative to depleted WT

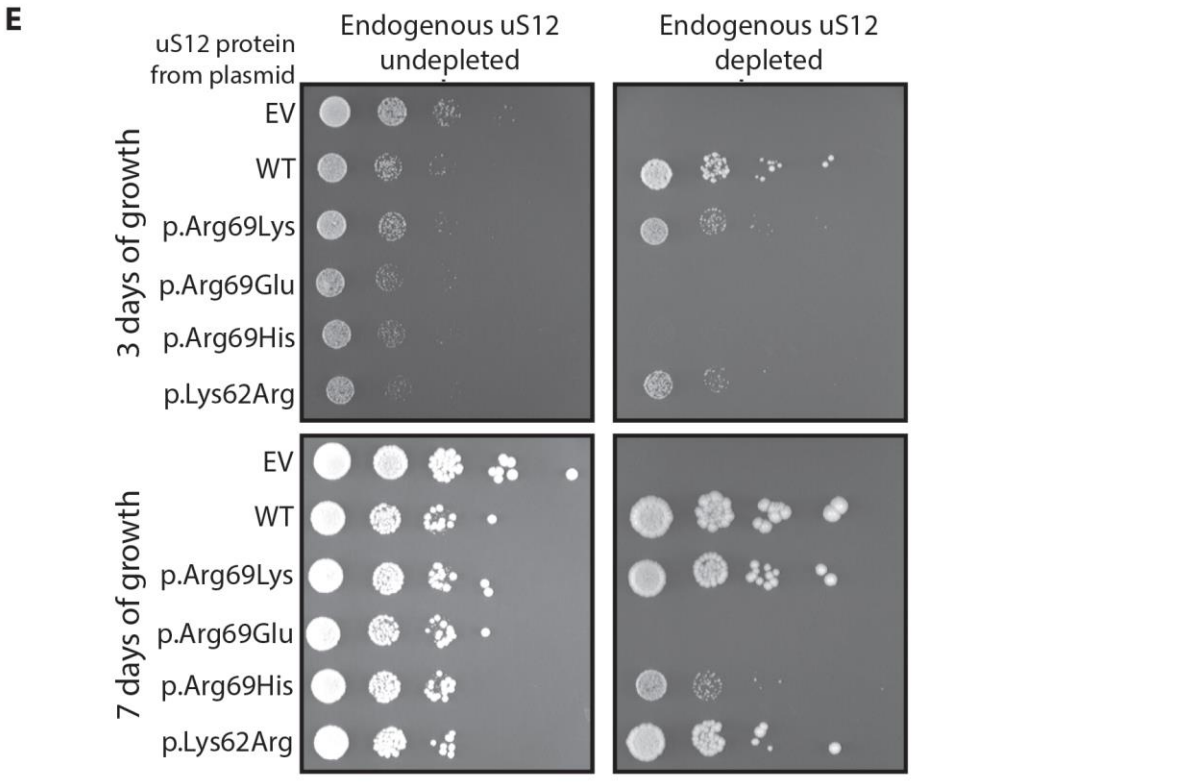
E
uS12 protein from plasmid
Endogenous uS12 undepleted
Endogenous uS12 depleted
3 days of growth
EV
WT
p.Arg69Lys
p.Arg69Glu
p.Arg69His
p.Lys62Arg
7 days of growth
EV
WT
p.Arg69Lys
p.Arg69Glu
p.Arg69His
p.Lys62Arg

Figure 2

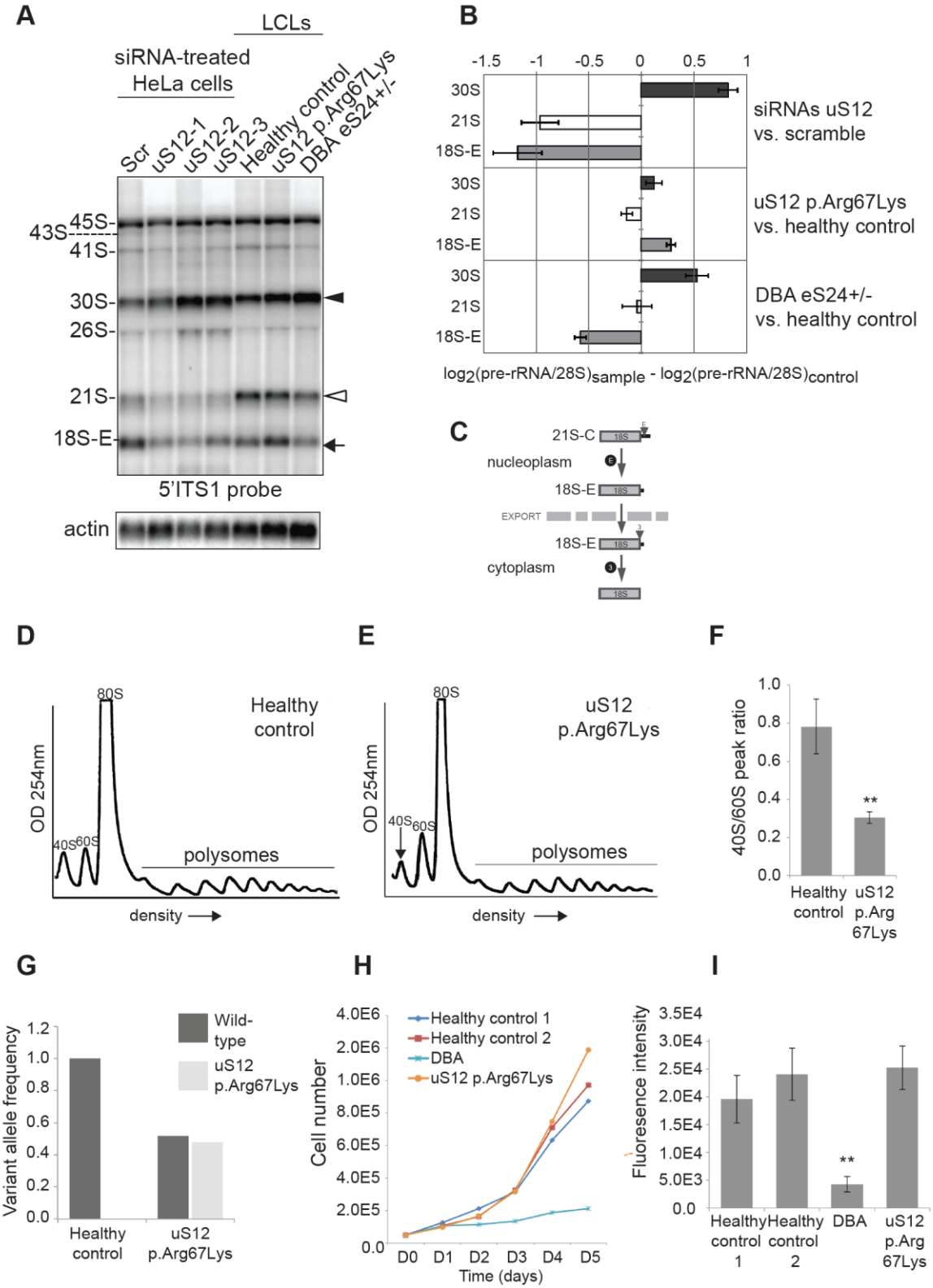
A
LCLs
siRNA-treated HeLa cells
Scr
uS12-1
uS12-2
uS12-3
Healthy control
uS12 p.Arg67Lys
DBA eS24+/-
43S
45S-
41S-
30S-
26S-
21S-
18S-E-
5'ITS1 probe
actin
B
-1.5
-1
-0.5
0
0.5
1
30S
21S
18S-E
siRNAs uS12 vs. scramble
uS12 p.Arg67Lys vs. healthy control
DBA eS24+/- vs. healthy control
log2(pre-rRNA/28S)sample - log2(pre-rRNA/28S)control
C
21S-C
nucleoplasm
18S-E
EXPORT
18S-E
cytoplasm
D
80S
Healthy control
OD 254nm
40S
60S
polysomes
density
E
80S
uS12 p.Arg67Lys
OD 254nm
40S
60S
polysomes
density
F
40S/60S peak ratio
1.0
0.8
0.6
0.4
0.2
0.0
**
Healthy control
uS12 p.Arg 67Lys
G
Variant allele frequency
1.2
1.0
0.8
0.6
0.4
0.2
0.0
Wild-type
uS12 p.Arg67Lys
Healthy control
uS12 p.Arg67Lys
H
Cell number
4.0E6
2.0E6
1.0E6
8.0E5
6.0E5
4.0E5
2.0E5
0.0
Healthy control 1
Healthy control 2
DBA
uS12 p.Arg67Lys
D0
D1
D2
D3
D4
D5
Time (days)
I
Fluorescence intensity
3.5E4
3.0E4
2.5E4
2.0E4
1.5E4
1.0E4
5.0E3
0.0
**
Healthy control 1
Healthy control 2
DBA
uS12 p.Arg 67Lys

Figure 3

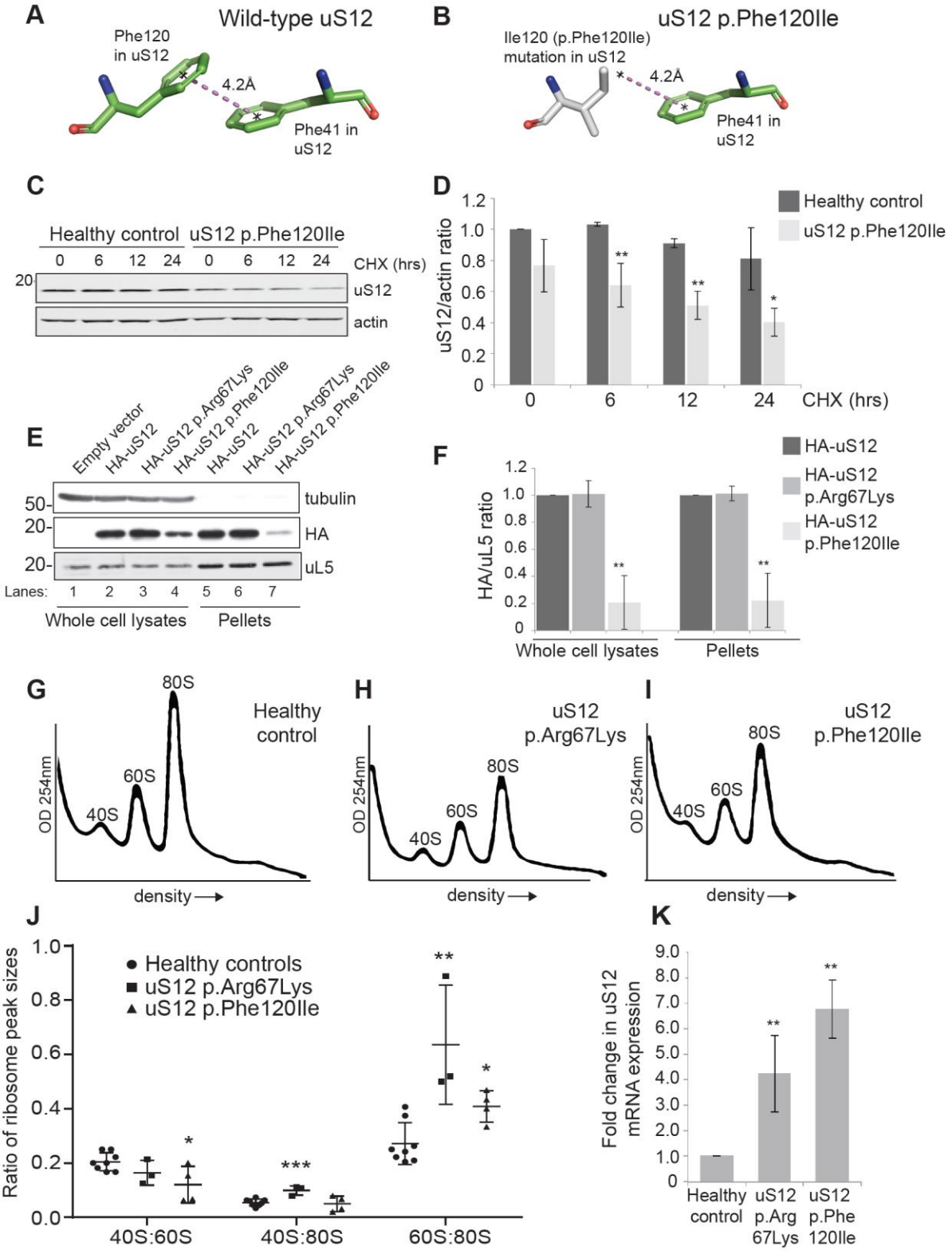
A
Wild-type uS12
Phe120 in uS12
4.2Å
Phe41 in uS12
B
uS12 p.Phe120Ile
Ile120 (p.Phe120Ile) mutation in uS12
4.2Å
Phe41 in uS12
C
Healthy control
uS12 p.Phe120Ile
0 6 12 24 0 6 12 24 CHX (hrs)
20
uS12
actin
D
uS12/actin ratio
Healthy control
uS12 p.Phe120Ile
CHX (hrs)
E
Empty vector
HA-uS12
HA-uS12 p.Arg67Lys
HA-uS12 p.Phe120Ile
50-
20-
20-
tubulin
HA
uL5
Lanes: 1 2 3 4 5 6 7
Whole cell lysates
Pellets
F
HA/uL5 ratio
HA-uS12
HA-uS12 p.Arg67Lys
HA-uS12 p.Phe120Ile
Whole cell lysates
Pellets
G
Healthy control
80S
60S
40S
OD 254nm
density
H
uS12 p.Arg67Lys
80S
60S
40S
OD 254nm
density
I
uS12 p.Phe120Ile
80S
60S
40S
OD 254nm
density
J
Ratio of ribosome peak sizes
Healthy controls
uS12 p.Arg67Lys
uS12 p.Phe120Ile
40S:60S
40S:80S
60S:80S
K
Fold change in uS12 mRNA expression
Healthy control
uS12 p.Arg 67Lys
uS12 p.Phe 120Ile

Figure 4

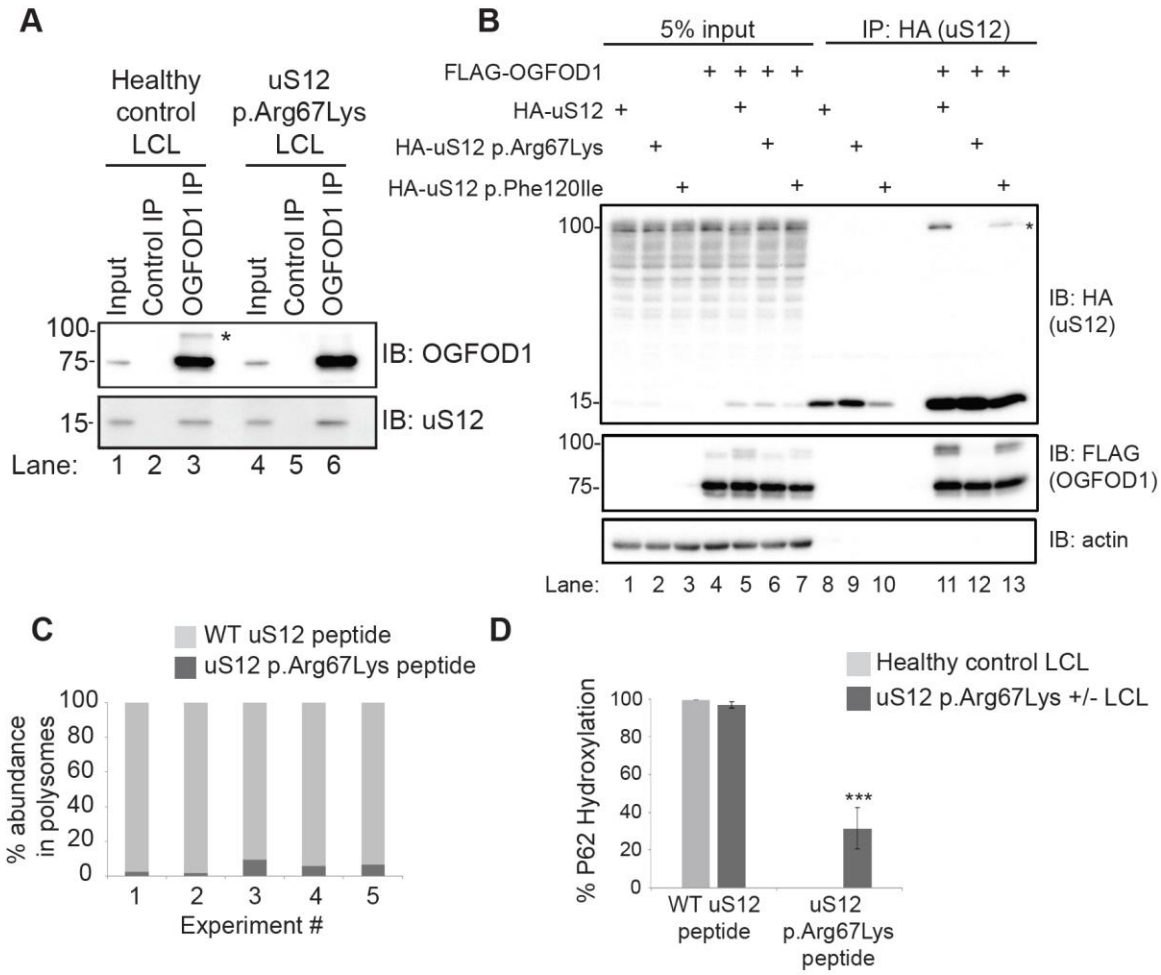
A
Healthy control LCL
uS12 p.Arg67Lys LCL
Input
Control IP
OGFOD1 IP
100-
75-
15-
IB: OGFOD1
IB: uS12
Lane: 1 2 3 4 5 6
B
5% input
IP: HA (uS12)
FLAG-OGFOD1
HA-uS12
HA-uS12 p.Arg67Lys
HA-uS12 p.Phe120Ile
IB: HA (uS12)
IB: FLAG (OGFOD1)
IB: actin
Lane: 1 2 3 4 5 6 7 8 9 10 11 12 13
C
WT uS12 peptide
uS12 p.Arg67Lys peptide
% abundance in polysomes
Experiment #
D
Healthy control LCL
uS12 p.Arg67Lys +/- LCL
% P62 Hydroxylation
***
WT uS12 peptide
uS12 p.Arg67Lys peptide

Figure 5

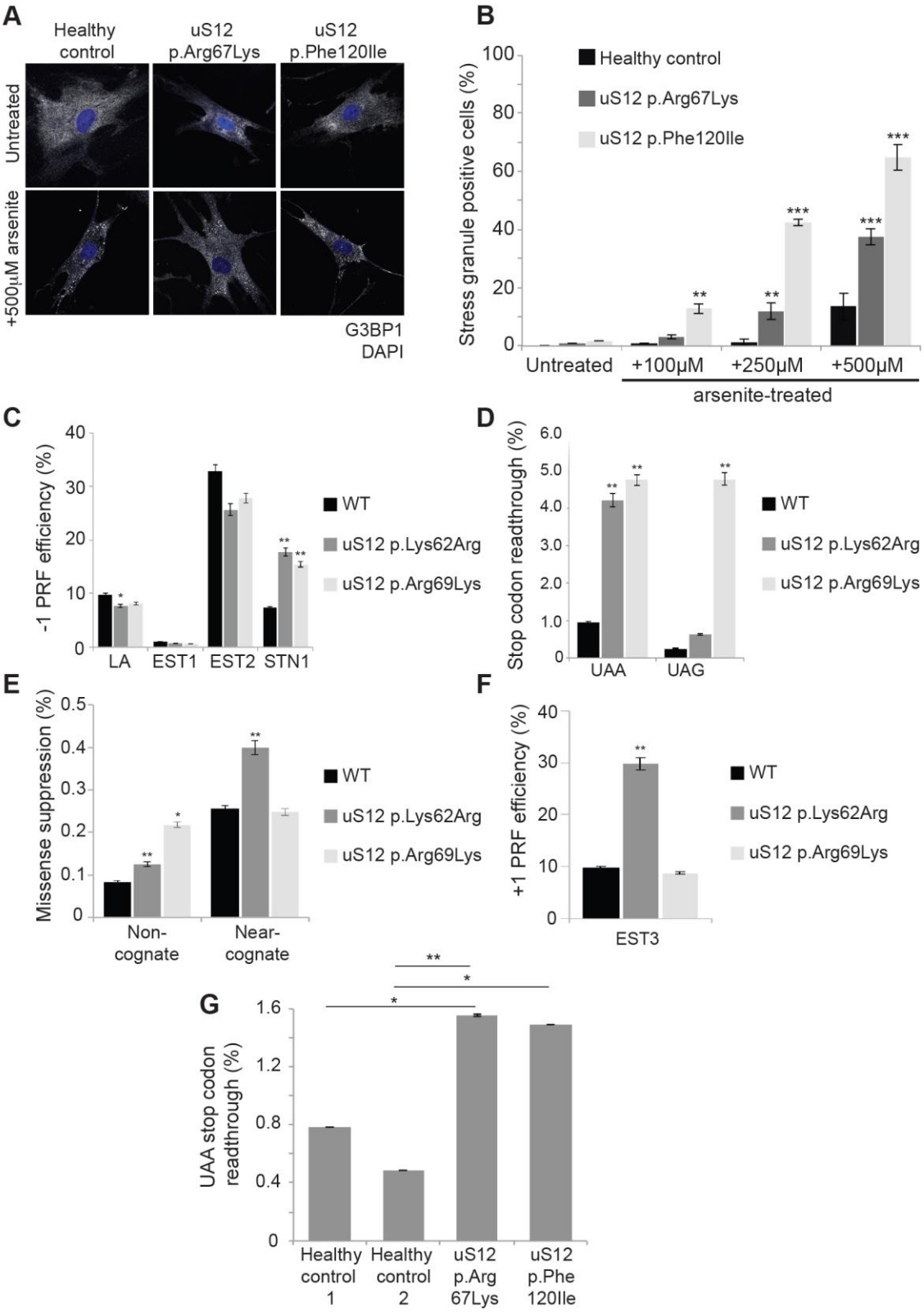
A
Healthy control
uS12 p.Arg67Lys
uS12 p.Phe120Ile
Untreated
+500μM arsenite
G3BP1
DAPI
B
Healthy control
uS12 p.Arg67Lys
uS12 p.Phe120Ile
Stress granule positive cells (%)
Untreated
+100μM
+250μM
+500μM
arsenite-treated
C
-1 PRF efficiency (%)
WT
uS12 p.Lys62Arg
uS12 p.Arg69Lys
LA
EST1
EST2
STN1
D
Stop codon readthrough (%)
UAA
UAG
E
Missense suppression (%)
Non-cognate
Near-cognate
F
+1 PRF efficiency (%)
EST3
G
UAA stop codon readthrough (%)
Healthy control 1
Healthy control 2
uS12 p.Arg 67Lys
uS12 p.Phe 120Ile